Digital position control of a closed-loop hydraulic system

Pekka Knuuttila

School of Engineering

Thesis submitted for examination for the degree of Master of Science in Technology.

Espoo 30.11.2015

Thesis supervisor:

Prof. Matti Pietola

Thesis advisor:

M.Sc. (Tech.) Sami Palokangas

Aalto University
School of Engineering

Author: Pekka Knuuttila

Title: Digital position control of a closed-loop hydraulic system

Date: 30.11.2015 Language: English Number of pages: 6+68

Department of Engineering Design and Production

Professorship: Engineering design

Supervisor: Prof. Matti Pietola

Advisor: M.Sc. (Tech.) Sami Palokangas

The design of safe and reliable digital control systems requires understanding phenomena that do not exist in continuous-time control systems. Neglecting this in the design process may cause significant unwanted behavior or even instability.

In this thesis, the digital position control of an existing closed-loop hydraulic system is studied by means of simulation. Models are developed for the hydraulic system, based on mathematical models of the system components, and for the digital controller based on the properties of digital control systems. The aim is to take into account the most important aspects of digital control.

Previously, the system has been successfully controlled by an analog controller. This thesis focused on the study of digital controllers with sample rates between 5 and 20 Hz. The performances of the analog and digital controllers were compared in various conditions, including model parameter variations and the presence of measurement noise. It was found that by an appropriate filtering and selection of simple control equations, the performances of the two controllers were practically equivalent.

Keywords: Digital control, quantization, sampled-data systems, discrete-time

Tekijä: Pekka Knuuttila

Työn nimi: Suljetun hydraulijärjestelmän digitaalinen asemasäätö

Päivämäärä: 30.11.2015 Kieli: Englanti Sivumäärä: 6+68

Koneenrakennustekniikan laitos

Professuuri: Koneensuunnittelu

Työn valvoja: Prof. Matti Pietola

Työn ohjaaja: DI Sami Palokangas

Turvallisten ja luotettavien digitaalisten säätöjärjestelmien suunnittelu vaatii ymmärrystä sellaisista ilmiöistä, joita ei esiinny jatkuva-aikaisissa säätöjärjestelmissä. Näiden ilmiöiden laiminlyöminen järjestelmän suunnittelussa saattaa johtaa järjestelmän epätoivottuun käyttäytymiseen tai pahimmassa tapauksessa jopa epästabiiliin järjestelmään.

Tässä työssä tutkitaan jo olemassa olevaa suljettua hydraulijärjestelmää ja sen digitaalista säätöä simuloinnin avulla. Hydraulijärjestelmän malli kehitetään sen komponentteja kuvaavien matemaattisten mallien pohjalta. Vastaavasti digitaaliselle säätimelle kehitetään malli perustuen digitaalisten järjestelmien ominaisuuksiin. Työn tavoitteena on tutkia digitaalisten säätöjärjestelmien tärkeimpiä ominaisuuksia ja niiden vaikutuksia.

Aikaisemmin järjestelmää on onnistuneesti ohjattu analogisella säätimellä. Työssä keskityttiin tutkimaan digitaalisia säätimiä, joiden näytteenottotaajuudet olivat välillä 5 Hz ja 20 Hz. Näiden säätimien suorituskykyä vertailtiin olemassa olevan analogisen säätimen suorituskykyyn. Suorituskykyjä vertailtiin useissa eri tilanteissa, mukaanlukien mallin parametrimuutokset ja mittauskohinan läsnäolo. Tulosten perusteella löydettiin, että sopivalla suodatuksella ja yksinkertaisilla ohjausyhtälöillä päästiin käytännössä vastaavaan suorituskykyyn.

Avainsanat: Digitaalinen säätö, kvantittuminen, diskreettiaikainen, näytteistys

Preface

I want to thank my thesis supervisor Prof. Matti Pietola for supervision and advice.

I wish to thank my thesis instructor Sami Palokangas for taking genuine interest in this thesis and for organizing regular meetings that provided me with essential information and motivation to complete this thesis. I am also grateful to Timo Heine for attending these meetings and for the effort to gather several documents which I needed during this thesis. I want also to thank Jussi Honkonen and Jussi Heikkinen for participating in the meetings and giving me advice and opinions.

Finally, I want to thank my parents and my family for the constant support.

Helsinki, 30.11.2015

Pekka Knuuttila

Contents

Symbols

Symbols

Latin letters

C_e	effective hydraulic capacitance
D_A	volume per load rotation
D_m	motor radial displacement
E	modulus of elasticity
f	frequency
f_{fbp}	antialiasing filter breakpoint
$F(\cdot)$	Fourier transformation
$G(s)$	continuous-time transfer function
$H(z)$	discrete-time transfer function
k_p	pump coefficient
$\mathbf{K}$	control law matrix
K_{hdt}	hydrodynamic torque coefficient
K_{sc}	scaling factor for load torque
K_A	load model numerator
L	leakage coefficient
p_p	pump double pole location
P	pressure
Q	volume flowrate
s	complex variable in s-plane
T_A	load side torque
T_m	motor side torque
T_{dm}	measurement delay
T_r	rise time
T_s	sampling period
u_c	control command
V	volume
$\mathbf{x}$	state vector
z	complex variable in z-plane

Greek letters

α_p	pump swashplate angle
β	bulk modulus
$\delta(t)$	Dirac delta function
θ_A	load angle
θ_f	filtered load angle measurement
μ	measurement noise average amplitude
ω_b	closed-loop bandwidth
ω_s	sampling angular frequency

1 Introduction

Digital computer controllers have become increasingly common in control systems as the price and reliability have improved dramatically [1]. Digital controllers are used in a great number of industries, and are applied in aircrafts, automobiles, oil refineries and paper machines [2], to name a few. Practically all control systems constructed today are based on computer control [3]. There are several reasons to this. Important advantages of digital controllers include flexibility of control programs [2], possibility of using control schemes that cannot be obtained with continuous-time controllers, low cost [3] and elimination of analog drift [4].

Although digital controllers are in many cases superior to analog controllers, the use of digital controllers introduce phenomena that are not found in analog control systems. Neglecting the existence of such phenomena can lead to harmful consequences such as degraded performance, instability and system failure. In order to design safe and reliable digital control systems, it is therefore essential to understand digital control.

Four key aspects of a digital control system are the sample rate, computer and converter word sizes, noise filtering and control algorithm. In general, the control system performance is degraded as either the sample rate or word size is lowered. However, increasing the sample rate increases the burden of the controller and greater computational power is required, which might increase the system costs or complexity. On the other hand, a good control algorithm might enable to decrease the sample rate without significantly decreasing the performance. One of the goals of digital control system design is to find control solutions with acceptable performance and costs.

It is sometimes the case that a well-functioning analog controller already exists. However, the advantages of digital controllers and the potential for augmented functionality might stimulate to explore the possibilities and challenges of replacing the existing analog controller. This is the background and motivation for this thesis. An existing closed-loop hydraulic system has been successfully controlled in the past by an analog controller. The system structure is introduced in Sec. 4.1.1.

The objective of this thesis is to predict and approximate the performance of the closed-loop hydraulic system when a digital controller is used instead of the analog controller. This thesis aims to account for the most important phenomena that exist in digital control systems. Since an optimal performance criteria has not been established nor is it particularly important, the performance obtained by the digital controllers is contrasted to the performance obtained with the existing analog control scheme. Therefore, the objective of this thesis is not to design an optimal control system but rather to design the simplest possible control system that results in equivalent performance. Two benefits of this approach are that positive results are more informative and that complexity is kept to a minimum.

In order to accomplish the objective of this thesis, a model that describes the dynamic behavior of the hydraulic system must be developed. The dynamics of the hydraulic components are modeled based on literature review. In addition to the hydraulic system model, a model must be developed for the digital controller

that captures the relevant phenomena such as measurement noise and delays. These models are then tested with various parameter configurations. The purpose of the testing is to determine the four key requirements for the digital control system: sample rate, word size, filtering and control algorithm.

This thesis is structured as follows. The second section covers the structure and properties of sampled-data systems. The third section considers theoretical aspects of digital control systems that are beneficial in understanding the system and interpreting the results. The fourth section focuses on the system modeling, where a theoretical basis for the hydraulic system model is presented. A SIMULINK® model and a linear state-space representation is developed and analyzed. The fifth section presents the simulation results of the system testing for different system configurations. These results are then interpreted in the sixth section and a final conclusion is provided.

2 Sampled-data systems

The purpose of this section is to investigate the structure and general properties of digital control systems. The goal is to understand digital control systems and to identify potential issues.

We will discuss topics such as sampling and sample rate selection, control methods, quantization, aliasing and dynamic effects of antialiasing filtering.

2.1 Operation

A *discrete-time signal* differs from a *continuous-time signal* in that the consecutive values are separated by a finite time interval. For both signals, the amplitude of the signal can be either discrete or continuous. A *digital signal* is one for which both time and amplitude are discrete [5]. The term *quantization* refers to the continuous amplitude being transformed into a discrete amplitude version.

A *sampled-data system* is a system with both discrete signals and continuous signals [2]. Therefore, a system where a continuous-time plant is controlled by digital logic or a digital computer is an example of a sampled-data system. The operation of a digital controller can be divided into three phases: sampling, digital processing and holding. A block diagram representation of a typical digital control system is presented in Fig. 2.1, where $r(t)$, $e(t)$, $u(t)$ and $y(t)$ are continuous-time signals and $e(k)$ and $u(k)$ are discrete-time signals.

Sampling and finite precision calculations introduce new phenomena to the control system, such as aliasing (covered in Sec. 2.3) and quantization (covered in Sec. 2.4). The analysis and design of digital controls is primarily concerned with taking account of the effects of the sampling period T and the quantization size q [2]. Sometimes the same design methods can be used for both continuous-time systems and sampled-data systems. If the sampling frequency is sufficiently large (30 or more times the system bandwidth) and the quantization effects very small (16-bit word size), digital signals are nearly continuous and continous methods can be used [2]. In a digital controller design technique called *emulation*, a continuous controller is simply replaced by a discrete equivalent of the continuous controller [2]. In the past, many industrial digital control systems were successfully designed using design techniques originally developed for continuous-time systems [8]. Therefore, the experience gained from a well-functioning continuous-time control system can provide valuable information to the design of a digital control system.

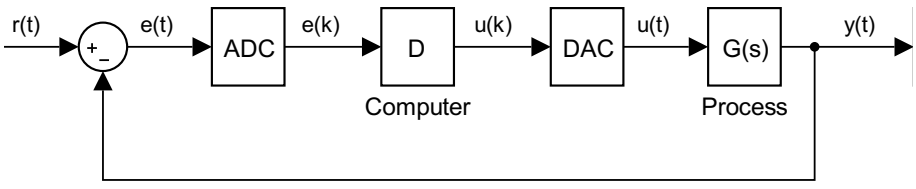

Figure 2.1: A block diagram of a computer-controlled system.

2.1.1 Sampling

A digital computer performs computations on digital data and therefore any analog measurement signal has to be converted into a digital representation before it can be processed by the computer. Such representation can be generated by executing three basic operations: *sampling*, *quantizing* and *encoding* [6], thus the name sampled-data system. A signal resulting from sampling is a discrete-time signal that (ideally) has the same values as the original signal at sampling instants. Therefore, the digital computer operates on discrete and quantized sequences of numbers instead of continuous-time and continuous amplitude signals. The resulting sequence of numbers is typically generated by means of *periodic sampling*, although other possibilities exist [5]. In periodic sampling one sample is taken every T_s seconds (the sampling period), i.e. T_s is a constant. The inverse, $f_s = \frac{1}{T}$, is called the *sample rate*). From now on periodic sampling will be referred to as sampling and it is the sampling method assumed throughout the rest of this thesis.

The sampling process can be represented mathematically by the so called *ideal sampler*. Consider a switch (normally open) that separates the receiving end from the input signal $f(t)$, which then closes for an instant of time every T_s seconds. During other times the value of the signal in the receiving end is 0. The *Dirac delta function* $\delta(t)$

$$\delta(t) = \begin{cases} +\infty & \text{if } t = 0 \\ 0 & \text{if } t \neq 0 \end{cases}, \int_{-\infty}^{+\infty} \delta(t)dt = 1$$

is used to represent the signal in the receiving end of the switch. If the switch is closed only once after, say k sampling periods, the resulting discrete-time signal is then simply $f^*(t) = f(t)\delta(t - kT_s)$. If the switch closes periodically, the resulting discrete-time signal is a sum of these signals. Given a continuous-time signal $f(t)$, the resulting discrete-time signal can therefore be represented mathematically as a sum of the instantaneous values of $f(t)$ multiplied by $\delta(t - kT_s)$ as follows

$$f^*(t) = \sum_{k=-\infty}^{\infty} f(t)\delta(t - kT_s) \tag{2.1}$$

where δ is the Dirac delta function and T_s is the sampling period. This is known as *impulse sampling*. We note that the instantaneous values are exact in their amplitude and in their spacing in the time domain. In control system applications it is often assumed that $f(t) = 0, \text{ if } t < 0$.

In a digital control system, sampling can be performed by an *analog-to-digital converter* (ADC), which acts on a physical variable such as an electrical voltage and converts it into a stream of numbers [2]. In practice, the sampling process is not ideal and errors are generated due to variations in sampling period (*jitter*), finite conversion time and quantization. Other important considerations in the selection of an ADC include linearity of quantization steps and limitations on sample rate [5]. Although the sampling period is not perfectly constant, measurements indicate that jitter typically ranges from hundreds of nanoseconds to tens of microseconds

for commercially available real-time controllers [9] and it is usually assumed to have negligible effects on control system performance [9, 10]. In contrast to the timeframes of jitter, the sampling periods we will be focusing later on in this thesis range from 50 to 200 ms. Furthermore, the quantization error is typically small and the ideal sampler model is acceptable for most engineering applications [10].

2.1.2 Digital processing

The control algorithm programmed into the computer calculates an output sequence based on the present and/or past values of the reference signal, received measurements and previous outputs. The behavior of a continuous linear system can be described by differential equations. In similar way, the behavior of a linear computer-controlled system can be described (at sampling instants) by linear *difference equations* [3]. Such a difference equation relates an input number sequence into a certain output number sequence that can be easily calculated by a computer. It can be expressed generally as

$$\begin{aligned} y(kT) + b_{m-1}y(kT-T) + \ldots + b_0 y(kT-mT) \\ = a_m u(kT) + a_{m-1}u(kT-T) + \ldots + a_0 u(kT-mT) \end{aligned} \tag{2.2}$$

where $y(t)$ and $u(t)$ are the output and the input at a time t, respectively. In other words, the next output value depends on present and/or past values according to the coefficients a and b. To simplify the notation we denote $y(kT)$ as $y[k]$ from now on. An important problem in the analysis of sampled-data systems is to find the relationship between the sequences $u[k]$ and $y[k]$, so that a proper control algorithm can be developed. This relationship between the discrete linear system input and output can also be described by the *discrete transfer function* based on the *z-transform* (introduced briefly in Sec. 3.2) or the *state-space representation*. We will give the discrete state-space representation of the system here. Given a continuous plant described by a state-space representation

$$\begin{aligned} \frac{d}{dt}\mathbf{x}(t) &= \mathbf{A}\mathbf{x}(t) + \mathbf{B}\mathbf{u}(t) \\ \mathbf{y}(t) &= \mathbf{C}\mathbf{x}(t) \end{aligned} \tag{2.3}$$

where $\mathbf{x}(t)$ is the system state vector and $u(t)$ is the input, the sequence $y[k]$ resulting from $u[k]$ can be obtained by *discretizing* the plant. Setting

$$\begin{aligned} \mathbf{\Phi} &= e^{\mathbf{A}T} \\ \mathbf{\Gamma} &= \int_0^T e^{\mathbf{A}\eta} d\eta \mathbf{G} \end{aligned} \tag{2.4}$$

and assuming zero-order hold (u(t) is constant between sampling instants) leads to a set of difference equations describing the plant at sampling instants [2]

$$\begin{aligned} \mathbf{x}[k+1] &= \mathbf{\Phi}\mathbf{x}[k] + \mathbf{\Gamma}\mathbf{u}[k] \\ \mathbf{y}[k] &= \mathbf{C}\mathbf{x}[k]. \end{aligned} \tag{2.5}$$

The model of the discrete-time system can thus be obtained by calculating $\mathbf{\Phi}$ and $\mathbf{\Gamma}$.

Returning to the block diagram of the computer-controlled system in Fig. 2.1, the purpose of the digital controller is to compute an output sequence $u[k]$ from an input sequence $e[k]$ based on the system dynamics (Eq. (2.5)), such that the error $e(t)$ (or the process output $y(t)$) will behave in an acceptable manner. Two design approaches that can be used in order to find an appropriate control algorithm are the *polynomial approach* and the *state-space approach* [3]. If the control algorithm in D is linear, then the difference equation describing the relationship between $e[k]$ and $u[k]$ takes the form [7]

$$\begin{aligned} u[k] = d_m e[k] + d_{m-1} e[k-1] + \ldots + d_0 e[k-m] \\ -c_{m-1} u[k-1] - \ldots - c_0 u[k-m]. \end{aligned} \tag{2.6}$$

or in the polynomial form [3, p. 166] (hence the name polynomial approach)

$$R(q)u[k] = T(q)u_c[k] - S(q)y[k] \tag{2.7}$$

where u_c is the command signal and $R(q)$, $T(q)$ and $S(q)$ are polynomials in the shift operator. In the polynomial approach, the design problem is then reduced to solving the so called *diophantine equation* [3].

In the state-space approach (using negative feedback), the control command $u[k]$ is obtained by taking the difference between the desired steady-state values and the product of a control law matrix and the state vector

$$u[k] = \mathbf{N_x r}[k] - \mathbf{K x}[k]. \tag{2.8}$$

where $\mathbf{K}$ is the control law, $r[k]$ is the reference signal and $\mathbf{N_x}$ is a vector that maps $r[k]$ to corresponding steady-state values. The closed-loop dynamic behavior is then determined by

$$\mathbf{x}[k+1] = (\mathbf{\Phi} - \mathbf{\Gamma K})\mathbf{x}[k] + \mathbf{\Gamma N_x r}[k]. \tag{2.9}$$

In order to obtain the desired closed-loop dynamics, the problem is then to find either the coefficients d_i and c_i in Eq. (2.6) or the control law $\mathbf{K}$. Eq. (2.9) assumes that all states are available for control calculations. However, generally not all the states are, nor need to be, measured. In an ideal situation the states could obtained accurately by calculating the states from Eq. (2.9) and using the calculated values for control. In practice the model is not perfect and the calculated states have to be corrected based on measurements. This is related to *estimator design*, which we will not be considering in this thesis.

2.1.3 Holding

The calculated output sequence is converted back into a continuous control signal by *decoding* and *holding* [7]. This is achieved by using a digital-to-analog controller (DAC), which is another source of quantization in a digital system. There are multiple ways to generate a continuous-time signal from a sequence of numbers.

Normally the control signal is just held constant between the conversions [3]. A method also known as the *zero-order hold*. The length of this hold period is also typically constant and in this thesis, we will assume that the hold period and the sampling period are the same and that they may assume new values only at multiples of the sampling period T. The resulting control signal will therefore be a staircase function.

2.2 Sample rate

Sample rate is one of the most important design parameters in a computer-controlled system. Sufficient sample rate is a prerequisite for successful digital data processing and it should be chosen so that the samples reflect the nature of the analog signal [10]. The sample rate should not be chosen either too large or too small. Too small sample rate will result in loss of information and degraded performance. The required minimum control loop bandwidth that is necessary for a good response sets the lower limit for the sample rate [7]. Increasing the sample rate generally increases both the performance and the unit product cost, although it may decrease the design costs due to less required design effort [2]. However, too large sample rate will also increase the load on the computer [3], whereas decreasing the sample rate allows more time for the controller to calculate the control calculations and decreases the required A/D conversion speed [2].

Thus, the selection of an appropriate sample rate is often a compromise between performance and cost. A logical choice for sample rate is the slowest sample rate that meets all performance spesifications [2].

Certain design examples in the literature have selected sample rates between 10 and 40 times the closed-loop bandwidth [11] (sampling multiple ω_s/ω_b) and [2] suggests using a sampling multiple of $20 \leq \omega_s/\omega_b \leq 40$ to achieve smoothness in the time response and limit the magnitude of the control steps. The required smoothness is highly subjective and depends on the application. Commands issued to hydraulic actuators are best kept fairly smooth and a low-pass filter is sometimes used between the ZOH and the hydraulic actuator [2]. For large sample rates (30 or more times the system bandwidth) and word sizes (16-bit), digital signals are nearly continuous and emulation approach can often be used [2].

As the reference signal can be received at any instant of time during the sampling period, there can be a delay up to one sampling period before the reference signal is received by the controller. Therefore, the rise time and settling time to a step response, for example, can vary a full sampling period depending on when the reference signal is issued with respect to the sampling instants.

To illustrate the relationship between sample rate and performance in a simple digital control system, consider a continuous second-order plant represented by a transfer function

$$G_p(s) = \frac{1}{s(s+1)}. \tag{2.10}$$

Closing the feedback loop, adding zero-order hold and a controller with a gain K, we get a sampled-data system presented in Fig. 2.2. For comparison the continuous

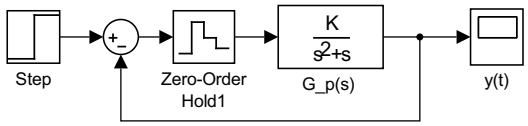

Figure 2.2: A sampled-data system.

system (without the zero-order hold) can be represented by a transfer function

$$G_s(s) = \frac{K}{s^2 + s + K}. \tag{2.11}$$

The controller in the sampled-data system is of course the discrete equivalent of the continuous controller and the performance is a function of the hold time T_s. As T_s increases, the performance is degraded and conversely, as T_s approaches zero, the difference in performance between the two systems gets smaller. The relationship between performance and sample rate depends also on the controller (in this case gain K). For example, the stability of the sampled-data system considered depends on both T_s and K. In more general terms, a second-order sampled system can be unstable when K is increased past a certain critical value even though the corresponding continuous system is stable for all values of gain K [1]. In this case the continuous system is indeed stable for all values of K, which is readily seen from the poles of it's transfer function

$$s^2 + s + K = 0, \text{ when } s = \frac{-1 \pm \sqrt{1 - 4K}}{2} \tag{2.12}$$

because $Re\{s\} < 0$, if $K > 0$, i.e. the poles of the system are in the left half-plane.

Plotting the unit step response of this system with different T_s and using the continuous response as a reference, we find significant differences in the responses as shown in Fig. 2.3. We observe that increasing the sampling period increases

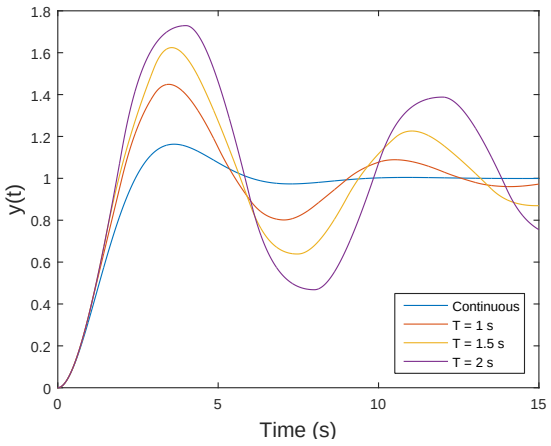

Figure 2.3: Effect of the sampling period with identical controller gains.

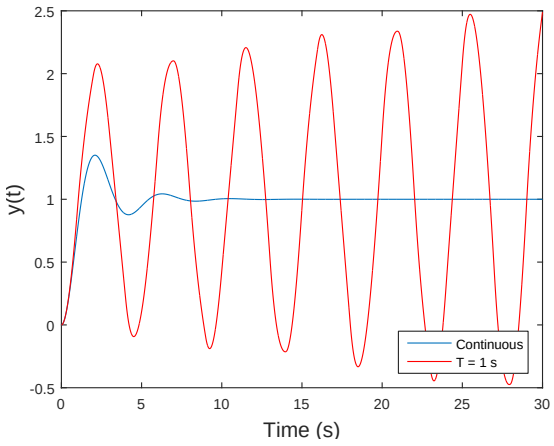

Figure 2.4: Instability with gain K = 2.5, $T_s = 1$ s.

settling time and overshoot. Moreover, it negatively influences stability as a function of feedback loop gain. For example, when $T = 1\ s$, the sampled system ceases to be stable when $K > 2.39$. A detailed analysis of this can be found in [1]. The instability becomes increasingly evident as the gain exceeds the critical value, which is illustrated clearly in Fig. 2.4., for K = 2.5.

To show that an appropriate selection of control may enable to reduce the sample rate while retaining desirable performance, we use the state-space approach to control the system with sampling periods $T_s = 1$ s and $T_s = 2$ s. The state-space representations of the discretized plants are

$$T_s = 1\ s \rightarrow \dot{\mathbf{x}} = \begin{bmatrix} 1 & 0.6321 \\ 0 & 0.3679 \end{bmatrix} \mathbf{x} + \begin{bmatrix} 0.3679 \\ 0.6321 \end{bmatrix} u[k]$$

$$T_s = 2\ s \rightarrow \dot{\mathbf{x}} = \begin{bmatrix} 1 & 0.8647 \\ 0 & 0.1353 \end{bmatrix} \mathbf{x} + \begin{bmatrix} 1.135 \\ 0.8647 \end{bmatrix} u[k] \tag{2.13}$$

$$y = \begin{bmatrix} 1 & 0 \end{bmatrix} \mathbf{x}$$

where the states of the state vector $\mathbf{x}$ are position and velocity. Selecting an appropriate control law $\mathbf{K} = \begin{bmatrix} 0.632 & 0.632 \end{bmatrix}$ results in the responses shown in Fig. 5.38. Hence, we see the importance of the control law.

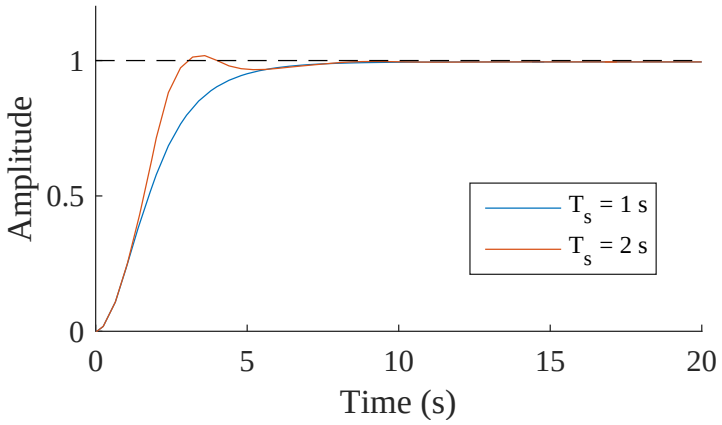

Figure 2.5: Digital control using state-space approach and pole placement.

2.3 Aliasing and antialiasing filtering

All physical waveforms encountered in engineering practice are Fourier transformable [6]. Therefore, any measured time signal $f(t)$ can be represented by a sum of sinusoidals. The *two-sided spectrum* of a signal, that represents the sinusoidal-type components in $f(t)$, can be obtained by the *Fourier transform* [6] given by[1]

$$F(\omega) = \mathcal{F}[f(t)] = \int_{-\infty}^{\infty} f(t)e^{-j\omega t}dt \tag{2.14}$$

where ω is angular frequency. From these transforms one important quantity is obtained, which is the *bandwidth* of a signal. There are many definitions for bandwidth, but in engineering definitions the bandwidth of a signal is the width of a positive frequency band [6].

Returning to the impulse sampled signal in Eq. (2.1), it can be shown (by Fourier transformation) that the spectrum of an impulse sampled signal is

$$F_s(\omega) = \frac{1}{T_s}\sum_{n=-\infty}^{\infty} F(\omega - n\omega_s) \tag{2.15}$$

where w_s is the sampling angular frequency and $F(\omega)$ is the Fourier transform of the original signal. An important result can be obtained from this equation. Eq. (2.15) shows that the spectrum of an impulse sampled signal is a superposition of the original spectra centered in integer multiples of w_s. If $w_s < 2\omega_b$, where ω_b is the bandwidth of the original signal then there is overlapping between the superposed spectra. This is a condition known as *folding*. If $w_s > 2\omega_b$, the spectra do not overlap and the original signal can be reconstructed using an ideal low-pass filter. This can be stated more formally. The *sampling theorem* sets a theoretical lower bound for the sampling rate necessary for a given bandlimited signal [10] (a signal for which the Fourier transform is zero above a certain frequency). The sampling theorem states that the original function $f(t)$ can be reconstructed from it's discrete-time waveform (Eq. (2.1)), if and only if the sampling angular frequency $2\pi\omega_s = \frac{1}{T_s}$ satisfies the condition [10]

$$\omega_s > 2\omega_b \tag{2.16}$$

where ω_b is the bandwidth of the signal. This means that no information is lost in the sampling process.

However, an absolutely time limited signal cannot be absolutely bandlimited and vice versa [6] and since all of the signals in engineering practice are time limited, they cannot also be bandlimited. When considering the sampling theorem, this raises a question about the required sample rate, as a physical signal cannot be reconstructed from it's discrete-time representation regardless of the (finite) sample rate. The resolution to this issue is related to the amplitudes of the different frequency components. Indeed, if the amplitude spectrum is negligible above a certain

[1] If the time signal $f(t) = 0$, when $t < 0$, the Eq. (2.14) is equal to the Laplace transform with the substitution $s = j\omega$.

level, the signal is bandlimited for all practical purposes [6, 10]. The signal then has an *effective bandwidth*, ω_m. The purpose of filtering in a digital control system is to attenuate undesired frequencies and reduce the effective bandwidth of the signal.

When a signal is sampled at a lower frequency than that in Eq. (2.16), the sinusoids of higher frequencies than $\frac{1}{2}f_s$ will appear at certain lower frequencies after sampling. The frequencies that appear at the same frequency after sampling are called each other's *aliases*. It can be seen directly from the spectrum of the impulse sampled signal in Eq. (2.15) that the aliases are found from

$$\omega_n = \omega_1 + n\omega_s \tag{2.17}$$

where ω_1 is the frequency that the frequency ω_n will appear on when sampled and ω_s is the sampling angular frequency. The frequencies ω_n and ω_1 cannot be distinguished from one another based on the sampled values and are called aliases of one another [2].

Considering Eq. (2.15), we see that the resulting spectrum is one where the frequency components of the original signal are added to the corresponding frequency component in the sampled spectrum. To illustrate how aliasing can be seen by a control system, we (impulse) sample a signal (true signal) that has the frequency components (unity amplitude) 1, $1 + w_s$ and $1 - w_s$, where $w_s = 10 \cdot 2\pi \ rad/s$ ($T_s = 0.10$ s) is the sampling angular frequency. The result is shown in Fig. (2.6), where two very different signals appear to be identical to the control system. In this particular case where the frequency components are in phase, the amplitude of the equivalent signal is the sum of the amplitudes of it's aliases, i.e. $1 + 1 + 1 = 3$. In this case, changing the amplitudes of the individual components may change the appearance of the true signal radically, but the effect to the equivalent signal is merely to change it's amplitude.

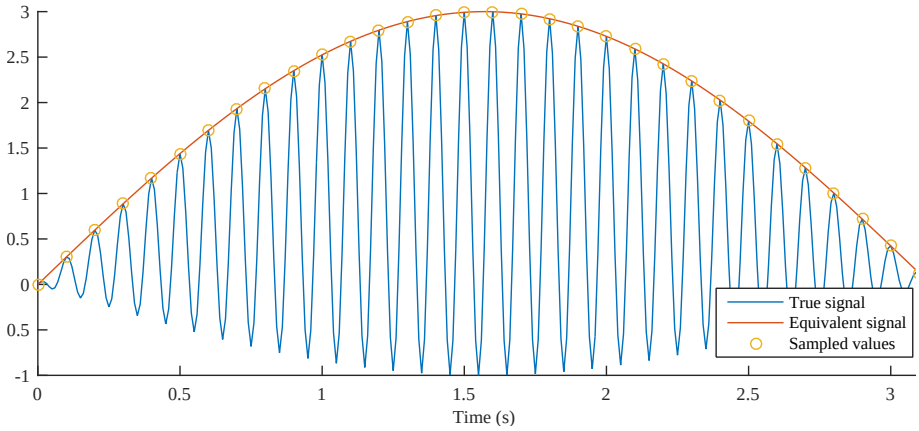

Figure 2.6: Aliasing of signals as seen by the control system.

From Fig. (2.6), the effect of reference signal aliasing is clear. The system behaves as if the reference signal was of a lower frequency. It is perhaps more interesting to study the effects of feedback signal aliasing and in particular the behavior of the

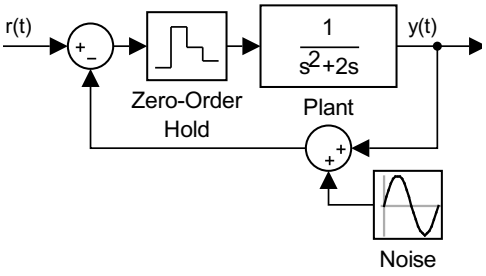

Figure 2.7: Sampled second-order system with measurement noise.

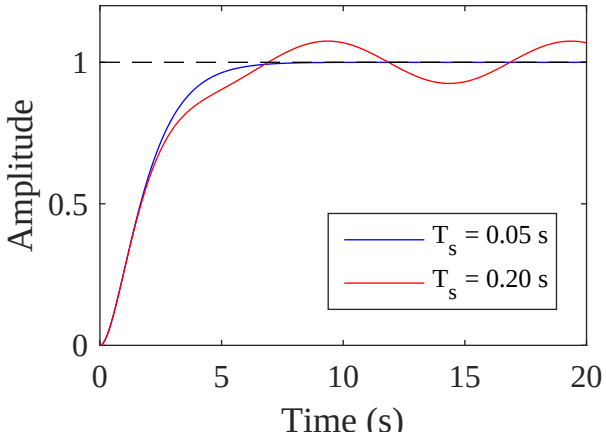

Figure 2.8: Influence of measurement noise to step responses with different sampling periods.

sampled system in the presence of measurement noise. Many real-life systems are low-pass filters in that they attenuate higher frequencies and do not react strongly to higher frequencies. However, as we saw, when a higher frequency signal is aliased it appears to be of a lower frequency, in which case the effects may be significant. Therefore, a very high-frequency signal that wouldn't have any measurable effects in an analog system can be detrimental in a sampled system. The problem is particularly serious if there are periodic high-frequency components [3]. For these reasons it is necessary to filter analog signals in a digital control system [3].

As an example, consider a second-order closed-loop control system (shown in Fig. 2.7) that is sampled at sampling periods $T_s = 0.05$ s and $T_s = 0.20$ s. The measurement noise is (for illustrative purposes) a $f_n = 9.9$ Hz sinusoidal signal with amplitude $A = 0.1$. At $f = 9.9$ Hz, the gain of the plant is approximately $|G(j2\pi f)| = -72$ dB. Since the sampling frequencies are $f_{s1} = 20$ Hz and $f_{s2} = 5$ Hz, we see that aliasing occurs only for the smaller sample rate. By Eq. (2.17), these aliases will appear at 4.9 Hz and -0.1 Hz for f_{s2}. At $f = 10$ Hz the gain is still about -72 dB, so the noise should not have any effect to the system for f_{s2}. However, at $f = 0.1$ Hz the gain is only about $|G(j2\pi f)| = -2.5$ dB and the consequences are apparent in the step responses, shown in Fig. 2.8. For $T_s = 0.20$ s, the high-frequency noise has aliased into a low frequency that significantly effects the system performance.

There is also the possibility that there exists frequencies in the signal that the samples do not show at all. These are called *hidden oscillations* [2]. If w_1 in Eq. (2.17) is set to $w_1 = 0$ rad/s, we find all the frequencies w_n that will appear as a DC-gain when sampled, the magnitude being dependent on the phase. If the phase happens to be such that the DC-gain is zero and the samples do not show the oscillation.

If the frequency components of the measurement noise are significantly higher than the important frequencies in the system, then the noise may be attenuated

by filtering the measured signal before sampling without significantly degrading the dynamic performance of the system. The filter for such purpose is called *antialiasing filter*. This filter is placed to precede the sampling. Antialiasing filters are low-pass filters and the simplest transfer function is [2]

$$G_f(s) = \frac{\omega_f}{s + \omega_f} \tag{2.18}$$

where ω_f is the filter breakpoint. In addition to this simple filter, there exists many types of more complex antialiasing filters. A standard second-order filter is [3]

$$G_f(s) = \frac{\omega_f^2}{s^2 + 2\zeta\omega_f s + \omega_f^2}. \tag{2.19}$$

Higher-order filters are obtained by cascading first- and second-order systems [3] and are used in order to obtain better high-frequency attenuation with minimum low-frequency phase lag [2].

The design goal is to select antialiasing filter so that the noise above $\omega_s/2$ is attenuated enough not to be detrimental to the control-system performance [2]. The gain of the filter in Eq. (2.18) can be calculated for a specific frequency from

$$|G_f(j\omega)| = \Big|\frac{\omega_f}{j\omega + \omega_f}\Big|. \tag{2.20}$$

If we now consider the noise ω_n present in the previous example and select the filter breakpoint to be at $\omega_f = 2\pi 5$ rad/s (5 Hz), we have, by Eq. (2.20)

$$|G_f(j\omega_n)| = -21.6 \text{ dB} \tag{2.21}$$

so the noise amplitude should be about 10 times less than without filtering. Plotting the step responses (Fig. 2.9) again for $T_s = 0.20$ s, we see that in this case the filtering virtually eliminates the effects of the measurement noise. Furthermore, the filter breakpoint is high enough compared to the plant dynamics not to degrade the system performance, even though the controller was unchanged.

However, if the filter breakpoint $\omega_f = 2\pi f_f$ is selected too low and not accounted for in the controller design, the system performance will eventually be degraded or even become unstable, due to phase lag introduced by the filter. Indeed, the effects of a filter can be conveniently approximated by a delay [3]. Fig. 2.10 shows the step responses of the system with $T_s = 0.20$ s and filter breakpoints $f_f = 5$ Hz, $f_f = 1$ Hz, $f_f = 0.5$ Hz and $f_f = 0.25$ Hz. As we saw, at 5 Hz the filtering has a negligible effect to performance. But as the breakpoint is lowered, a small overshoot will occur when $f_f = 0.5$ Hz and at $f_f = 0.25$ Hz there is already significant overshoot. To avoid these problems, two design procedures suggested by [2] are to either select the filter breakpoint sufficiently higher than the system bandwidth so as not significantly alter system stability and ignore it in the design, or to allow significant phase lag from the filter and design the control with prefilter included. For interested readers, this procedure is detailed in [12].

In conclusion, antialiasing filtering reduces (or in the best case completely eliminates) the effects of measurement noise, but may in some cases also degrade the dynamic response of the system if not accounted for in the design.

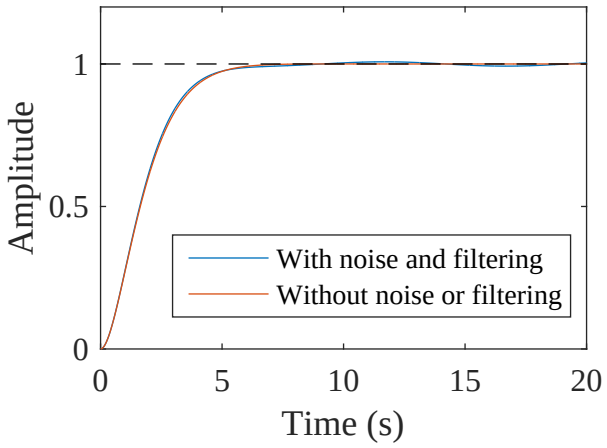

Figure 2.9: $T_s = 0.20$ s.

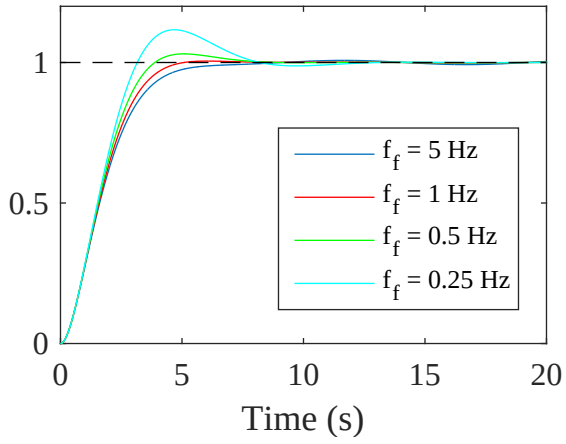

Figure 2.10: $T_s = 0.20$ s.

2.4 Quantization

Quantization occurs when physical quantities are represented numerically [16]. When a continuous set of numbers is represented by a finite number of binary digits, the resulting numbers will be separated by a certain finite interval that depends on the number of bits used. *Precision* is the accuracy with which a quantity is stated and is limited in computers and analog-to-digital converters by the number of binary digits used [1]. In some cases the precision limitations can be neglected altogether. This is the case if the amplitude of the signal is small relative to the quantization error [1]. For example the effect of quantization is typically not noticeable if 32-bit word size is used [2].

Two typical ways quantization can occur are *truncation* and *round-off*. Truncation occurs when the least significant bits are left out, while in the round-off the process is the same as with base 10 numbers [2]. Digital computers typically use round-off rather than truncation, [2] and we focus on round-off in this thesis.

Quantization is a special type of nonlinearity in digital control systems that, due to inaccurate representation of numbers, affects the control system in two principal ways. First, the variable values such as the state variables in the difference equations are not exact and thus errors will be introduced to the output. Second, the coefficients in the difference equations might not be exact and the computer will solve a slightly different equation than it was intended to solve. [2]

There are many ways to represent numbers in digital computers (e.g. fixed-point representation, floating point representation). One way is to use the floating-point format standardized by IEEE. A floating-point number has the form [15]

$$y = \pm m \cdot \beta^{e-t} \tag{2.22}$$

where m is the significand, β is the base, e is the exponent range and t is the precision. A thorough discussion of the subject can be found in [15], but for our purposes a simple consideration of the precision and range is sufficient. Given a certain finite number of bits, there will be a trade-off between range and precision depending on

how the bits are divided. For example, in the half-precision floating-point format (IEEE 754), 1-bit is reserved for the sign, 5-bits for the exponent and 10-bits for the significand. The precision by which a certain number can be represented depends on how far/close the number is from/to zero. This is relevant to digital control systems if, for example, there are large and small numbers (relative to the word size) in the plant model which is used to approximate the system states. This might result in inaccurate coefficients in the difference equations and must be considered when choosing the word size and control algorithm.

The stability of a quantized feedback system is unaffected by the presence of the quantizer [16, 17]. The effect of quantization is to inject a bounded noise which cannot cause an unbounded output in a stable system, but may cause stable-amplitude limit cycles [16]. The effects of this bounded noise can be analyzed in several different ways. A detailed description of these effects leads to a complicated nonlinear model that is very difficult to analyze [3]. Fortunately, such analysis is rarely necessary and often crude estimations are sufficient. For example, in a linear system the maximum error due to quantization can be easily calculated by using the worst-case method of Bertram presented in [17]. Using this method, the upper bound of the error can be found by simply replacing every quantizer with a unit gain element plus an input which is equal in magnitude to the greatest error possible in the element [17].

It is the existence of the stable-amplitude limit cycles and the dynamic effects of the bounded noise that we will be investigating in the results section (see Sec. 5).

2.5 Motion controllers

As we have seen, designing and constructing computer-controlled systems requires consideration of several factors. Due to the vast number of applications that require a controller, there is demand for simple, low-investment control solutions that can in some cases reduce design and unit product costs.

As a result, several companies currently offer products containing the required controller hardwares and controller design softwares. These products are commonly called *motion controllers*. Examples of companies that currently provide these products are National Instruments, Delta Computer Systems and ACS Motion Control.

The functionality that can be achieved with these controllers include PID loop control with feedforwards for velocity, acceleration and jerk [13], supervisory control and trajectory generation [14].

3 Control theory

3.1 Linear and nonlinear systems

A system is called a *linear system* if it satisfies the properties of superposition and homogeneity [1]. If we denote a certain system by an operator that maps an input signal $x_n(t)$ into an output signal $y_n(t)$ by $T\{\cdot\}$, then the system is linear if and only if the following conditions are fulfilled

$$T\{x_1(t) + x_2(t)\} = T\{x_1(t)\} + T\{x_2(t)\} = y_1(t) + y_2(t) \tag{3.1}$$

$$T\{kx(t)\} = kT\{x(t)\} = ky(t) \tag{3.2}$$

The two equations mean that the system satisfies the *additive property* and the *scaling property* [5], respectively. The final response can thus be found by adding the individual responses (taken separately) together. From Eq. (3.2), it is clear that the character of the response does not change with respect to the magnitude of the input, but is different merely in amplitude. Furthermore, the properties of a linear system remain unchanged regardless of the operating point. If the response of a linear system is the same regardless of the instant of time that the input signal was introduced, the system is called a *linear time-invariant* system. These properties enable the use of many powerful tools of analysis. Control engineering is based on the foundations of linear system analysis and feedback theory [1].

The additive property of a linear system implies that responses and effects of certain phenomena such as noise can be considered separately and merged together later. Two such examples relevant to this thesis are the measurement noise and quantization effects. The total response is a superposition of the ideal model response and response to disturbances.

A system that violates the properties of additivity or scaling in any condition is called a *nonlinear system*. As a result, the analysis of nonlinear systems is much more difficult and often focuses on quite specific problems. In reality all physical systems are nonlinear to some extent. Several performance phenomena are directly attributable to system nonlinearities, yet no general nonlinear theory exists [19]. A closed-form analytical solution is usually impossible to obtain for a nonlinear system [20] and in fact, even for a simple pendulum, the closed-form solution is very difficult to obtain [2]. The design of nonlinear control systems is also often challenging. This is especially true for discrete-time systems, for which the design is often yet more complicated than the design for nonlinear analog systems [10].

Multiple approaches exists that sometimes enable to overcome the difficulties encountered in nonlinear system design. Less insight is gained if only a nonlinear model of the system is used throughout the design process [2]. Two valuable tools are *linearization* and *computer simulation*. Even though all real systems are nonlinear to some extent due to saturations, most systems can be approximated to be linear (i.e. linearized) within a certain range of operating points. This is done by using the first-order terms in Taylor series expansion of the system about an operating point. The performance can then be calculated for every operating point using the tools

of feedback theory and linear system analysis. In a computer simulation, numerical methods are used to obtain numerical solutions. It is the only general method to find solutions to arbitrary nonlinear differential and difference equations [2]. While it is one of the most important tools in control engineering, it can only obtain solutions for specific inputs, initial conditions and parameters [2] and does not prove anything about the general behavior. Therefore, it is often important to perform additional analysis with the aid of tools such as linearization.

In a linear system instability means that the output will increase without bounds. However, this cannot happen in a physical device since the output is always limited by saturations. This leads to an important concept in nonlinear systems known as *limit cycle*. An example of a limit cycle is a condition where the output oscillates with a fixed amplitude and frequency [19]. Sometimes a limit cycle will occur because of a single nonlinear element. Since nonlinear systems are difficult to study, approximate methods such as the *describing function* have been developed to study the existence of limit cycles due to nonlinear elements such as backlash and deadband [21]. The method can be also used for sampled systems, but the technique is much more refined [21] and we will resort to computer simulation in the study of limit cycles.

3.2 Discrete-time transfer function

When the discrete-time series of impulses in Eq. (2.1) is Laplace transformed, we have[2]

$$\mathcal{L}\{f^*(t)\} = \sum_{k=0}^{\infty} f(kT)e^{-ksT}, \tag{3.3}$$

and substituting $z = e^{sT}$ results in

$$\mathcal{Z}\{f(t)\} = \mathcal{Z}\{f^*(t)\} = \sum_{k=0}^{\infty} f(kT)z^{-k}, \tag{3.4}$$

which is a series of modulated impulses delayed by multiples of T. This is known as the *z-transform* of a signal. The z-transform is the counterpart of the Laplace transform for continuous-time signals and satisfies the linearity property [5]. Thus, the superposition principle holds.

For responses generated by linear systems, the infinite series in Eq. (3.4) can often be represented in a closed form, which is useful in the analysis of discrete-time systems. For example, if the time signal is $f(t) = 1$ (unit step), the z-transform is simply

$$\mathcal{Z}\{1\} = \frac{z}{z-1}. \tag{3.5}$$

Closed-form solutions exists also for exponentially decaying signals and for exponentially decaying sinusoids. These closed-form solutions can be manipulated algebraically. Indeed, if a function $H(z)$ represents the z-transform of a unit pulse response of a discrete-time system, the response of that system (in the z-plane) to a

[2]Throughout this text we will assume that $f(t) = 0$, when $t < 0$

signal represented by $U(z)$ will be $Y(z) = H(z)U(z)$. This can be shown to directly result from Eq. (3.3). If the solution is a ratio of polynomials in z (which is the case if a response of a system is generated by a linear difference equation [2]), the values of the signal corresponding to times kT can be calculated by polynomial long division. In the resulting polynomial, the coefficient for z^{-k} is the value of the signal at a time kT (according to Eq. (3.4)). We can now represent delays of multiples of T very conveniently just by multiplying the z-transform (or Laplace transform) of the signal by z^{-k}, where k is the number of delays.

If a continuous control signal is generated from the controller calculations using zero-order hold, what is the response of a linear continuous plant? If we are only interested in the values at sampling instants, this can be easily calculated. Zero-order hold means that the controller outputs a pulse of of width T and amplitude $u(kT)$ (the calculated control value at time $t = kT$). A pulse of width T and magnitude 1 (unit pulse) can be Laplace-transformed into

$$1 \cdot \frac{1 - e^{-sT}}{s}, \tag{3.6}$$

which is a step superposed by a negative step delayed by T. After multiplying this with the transfer function of the plant, we obtain the response in the s-plane

$$Y(s) = U(s)G(s) = 1 \cdot \frac{(1 - e^{sT})}{s} G(s) = 1 \cdot (1 - e^{sT}) \frac{G(s)}{s} \tag{3.7}$$

where $G(s)$ is the transfer function of the continuous-time plant. Substituting z, we have

$$Y(s) = 1 \cdot (1 - z^{-1}) \frac{G(s)}{s}. \tag{3.8}$$

If we are only interested in the values at sampling instants, we can transform $G(s)/s$ into z-plane and arrive at discrete-time transfer function for a plant controlled with zero-order hold

$$Y(z) = 1 \cdot (1 - z^{-1}) \mathcal{Z} \left\{ \frac{G(s)}{s} \right\}. \tag{3.9}$$

The expression right to 1 is equal to the unit pulse response and we denote this as $H(z)$. A delayed control order occurring at a time kT (delayed by k sampling periods) can be expressed as $z^{-k}u(kT)$. By superposition principle, the pulse trains resulting from these control orders can be added. Thus, we have

$$Y_r(z) = \sum_{k=0}^{n} u(kT) z^{-k} \cdot H(z) = U(z)H(z). \tag{3.10}$$

Given that $H(z)$ is the open loop transfer function, the closed-loop transfer function is found from (as with continuous systems)

$$G_{cl}(z) = \frac{H(z)}{1 + H(z)}. \tag{3.11}$$

In conclusion, if a linear continuous-time plant is controlled using the zero-order hold, the resulting response is a superposition of positive and negative step responses of different magnitudes and time-shifts (multiples of T) and the discrete-time transfer function of the plant is found from

$$H(z) = (1 - z^{-1})\mathcal{Z}\left\{\frac{G(s)}{s}\right\}. \tag{3.12}$$

The roots of the denominator in $H(z)$ are the poles of the transfer function and determine the dynamic behavior of the system. Partial fraction expansion can be applied to explore the contribution of different poles.

The fact that $H(z)$ is equal to the unit pulse response implies that the discrete-time transfer function of a linear (stationary) plant can be found by recording the unit pulse response at sampling instants.

3.3 Partial fraction expansion

Every rational function may be represented as a ratio of two polynomials as follows [22]

$$\frac{Q(x)}{f(x)} = \frac{B_0x^m + B_1m^{-1} + \ldots + B_m}{A_0x^n + A_1n^{-1} + \ldots + A_n}. \tag{3.13}$$

A fraction is called *proper* if the degree of the numerator is lower than that of the denominator [22]. It can be proved that every rational fraction can be represented as a sum of *partial fractions*, that is, as a sum of the following proper rational fractions

$$\frac{A}{(x-a)^k}, (k \in \mathbb{N}) \tag{3.14}$$

$$\frac{Ax + B}{(x^2 + px + q)^k}, (k \in \mathbb{N}) \tag{3.15}$$

Given that the roots[3] of $Q(x)$ are b_1, $b_2 \ldots, b_m$ and the roots of $f(x)$ are a_1, $a_2 \ldots, a_n$, we can express Eq. (3.13) as

$$\frac{\prod_{i=1}^{m}(x - b_i)}{\prod_{j=1}^{n}(x - a_j)}. \tag{3.16}$$

If Eq. (3.13) is proper, we can use partial fraction expansion to represent $Q(x)/f(x)$ as a sum of terms such as in Eq. (3.14) and (3.15), where the roots of the denominators are the roots (or poles of a transfer function) a_1, $a_2 \ldots, a_n$. If the root a_j is real, then the term in the sum is of the form in Eq. (3.14) and if the root a_j is complex, then it is of the form in Eq. (3.15).

[3]The roots may also be complex.

The above operation is frequently applied in the analysis of control systems. For example, a signal represented in s-plane or z-plane can be transformed into a form that can be converted into time domain using the Laplace and z-transform tables. The problem is then only to find the roots of $f(x)$. Although no general solution exists for polynomials of degree five or higher, approximate roots can be found algorithmically by using computers. This can be performed in MATLAB® by using the function **residue**.

The magnitudes of the coefficients A and B also play a role in the significance of a certain pole to the overall behavior.

3.4 Pole location analysis

It is easier to characterize the time functions using s-plane poles [10] and therefore it is useful to consider the relationship between the pole locations in the s-plane and the pole locations in the z-plane.

If the response $y[k]$ of a system is generated by a linear difference equation with constant coefficients, then the z-transform $Y(z)$ of that response can be expressed as a sum of two elementary terms [2] and more complex time functions can be reduced to these simpler terms by partial fraction expansion [10]. The two continuous-time signals corresponding to the s-plane and z-plane are

$$\begin{aligned} y_1(t) = e^{-at} &\rightleftarrows \mathcal{L}\{y_1(t)\} = \frac{1}{s+a} \\ y_1[k] = e^{-ak} &\rightleftarrows \mathcal{Z}\{y_1[k]\} = \frac{z}{z-e^{-ak}} \end{aligned} \tag{3.17}$$

$$\begin{aligned} y_2(t) = e^{-at}\sin\omega t &\rightleftarrows \mathcal{L}\{y_2(t)\} = \frac{\omega}{(s+a)^2+\omega^2} \\ y_2[k] = e^{-ak}\sin\ \omega k &\rightleftarrows \mathcal{Z}(y_2[k]) = \frac{\sin(\omega T)e^{-aT}z}{z^2-2\cos(\omega T)e^{-aT}+e^{-2aT}} \end{aligned} \tag{3.18}$$

Based on these time signals, the s-plane poles contain information about

- Exponential decay rate = $\mathrm{Re}\{s_{1,2}\}$
- Frequency of oscillation = $\mathrm{Im}\{s_{1,2}\}$

This implies that the nature of the signal can be estimated visually based on the location of a and ω in the s-plane.

From the roots of these transforms, it can be observed that in both cases the relationship between the roots is $z = e^{sT}$. Since both transforms represent the same signal, the poles between s-plane and z-plane map according to

$$z = e^{sT} = e^{(a+i\omega)T} = e^{aT}e^{i\omega T}. \tag{3.19}$$

Because z is a complex number, another way to represent it is the trigonometric form of a complex number

$$z = r(\cos\varphi + i\sin\varphi) = e^{aT}(\cos\omega T + i\sin\omega T) \tag{3.20}$$

where r is the modulus (or radius) and φ is the argument (angle). The real part in the s-plane[4] is then $a = \log_e(r)/T$ and the imaginary part is the angle $\omega = \tan^{-1}(\varphi)/T$.

Using Eq. (3.20) we may solve the pole locations in z-plane, map them to s-plane and interpret the pole locations in the s-plane. This enables to compare the poles of a discrete system to the poles of a continuous system, which we may know from experience to yield a good performance. This is the case in this thesis.

Note that the numerator is not always a constant and may contain a z. However, in z-plane, the addition of a pole or zero in the range of 0 to -1 to a system has only a small effect. However, a zero near z = +1 increases the system overshoot significantly, while a pole placed near z = +1 slows down the response and primarily increases the rise time. These effects are increased as z increases towards z = +1. [2] As an example, consider the two discrete-time transfer functions

$$\begin{aligned} H_1(z) &= \frac{0.2}{z^2 - 1.5z + 0.7} \\ H_2(z) &= \frac{0.17}{z^2 - 0.83}, \end{aligned} \tag{3.21}$$

where $H_1(z)$ has poles at $z_{1,2} = 0.75 \pm 0.37i$ and $H_2(z)$ at $z_1 = 0.83$. If $T = 1$ s, these poles map to s-plane as follows

$$\begin{aligned} z_{1,2} \rightarrow s_{1,2} &= -0.178 \pm 0.46i \\ z_1 \rightarrow s_1 &= -0.18 \end{aligned} \tag{3.22}$$

which are plotted in Fig. 3.1. The frequency of oscillation for $H_1(z)$ should be 0.46 rad/s (period $T = 13.66$ s) and for $H_2(z)$ there should not be oscillations at all. The corresponding responses are presented in Fig. 3.2, which confirms both of the claims. Furthermore, since the real parts are approximately equal, the settling times ($T_{0-90\%}$) are also close to each other.

For higher-order systems, partial fraction expansion can be used to obtain a sum of terms such as those in Eq. (3.21), which means that the response of a higher-order system is a sum of responses of simpler terms.

The understanding of how poles and zeros affect the time response helps the designer to understand the reasons why a certain response is the way it is [2]. We have seen that, as long as the zeros in the z-plane are within the range of 0 to -1, the poles determine majority of the dynamic behavior of the system. Therefore negative feedback control, and variation of system parameters in general, must somehow

[4]Although we will not be A stable system cannot have any poles in the right half-plane and therefore a must be nonpositive. Thus, the stability criteria in the z-plane is $|z| \leq 1$.

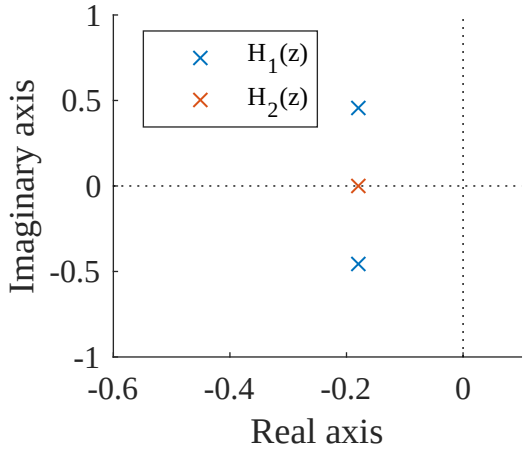

Figure 3.1: Discrete-time transfer function poles mapped to s-plane.

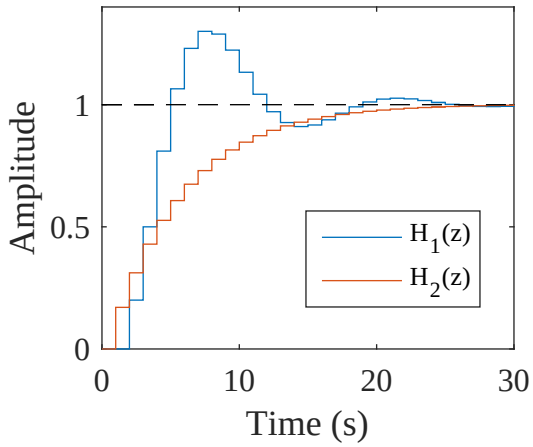

Figure 3.2: Discrete-time transfer function step responses.

change the poles of the system. The problem of controller design can thus be seen as placing the closed-loop system poles. Pole placement is a general approach to the design of single-input-single-output systems and many design techniques can be seen as pole placement [3]. If a system is controllable, there exists a suitable full-state control law $\mathbf{K}$ for every desired pole locations [7]. The formula that can be used to calculate $\mathbf{K}$ for the given poles is known as the *Ackermann's formula*. Of course, this is not the case for all control methods such as the P-controller (proportional controller), where the control law $\mathbf{K}$ has only one nonzero column. Since P-controller will be the main control method in this thesis, we will briefly consider, by way of example, the effect of gain variation in the control of two second-order plants described by the transfer functions

$$\begin{aligned} G_{p1}(s) &= \frac{1}{(s+a_1)^2+\omega_1^2} = \frac{1}{(s+1)^2+1} \\ G_{p2}(s) &= \frac{1}{(s+a_2)^2+\omega_2^2} = \frac{1}{(s+2)^2+1} \end{aligned} \tag{3.23}$$

with sampling periods $T_s = 0.25$ s and $T_s = 1$ s. These plants behave as damped spring-mass systems. The Figs. 3.3 and 3.4 show the effects of increasing controller gains in these spring-mass system. The controllers with larger sampling periods are more sensitive to the variation of the gain.

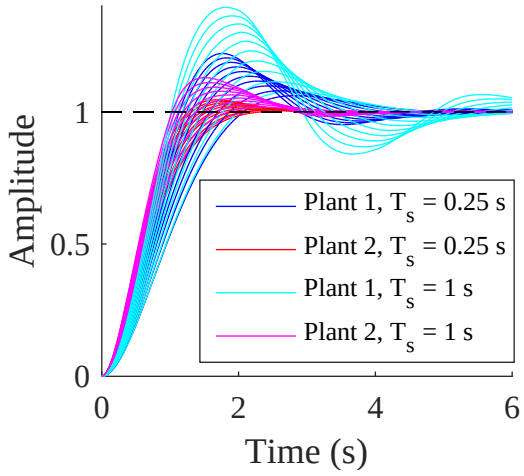

Figure 3.3: Step responses. Variation of controller gain K from 0.2 to 2.

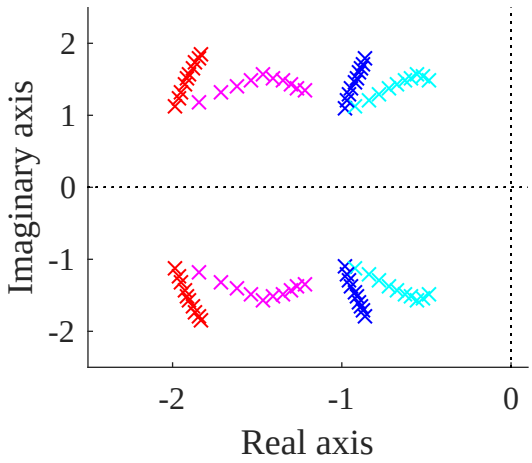

Figure 3.4: Pole locations. Variation of controller gain K from 0.2 to 2. Pole movement from left to right.

4 Modeling and model analysis

In this section, models for the hydraulic system and controllers will be developed. First, the hydraulic system structure is covered and mathematical descriptions for the hydraulic components are established based on literature and physical/mathematical reasoning. Second, a SIMULINK® model that is used in the system testing. Third, a state-space representation describing linearized dynamics (based on the differential equations) is developed and used for pole location analysis.

4.1 Hydraulic system

4.1.1 System structure

Including only the components relevant for this thesis, the hydraulic system consists of two variable displacement axial piston pumps, hydraulic lines, four motors, load and three control valves. The pump displacements are controlled by controllers that receive reference signal and angle measurement. A greatly simplified diagram of the system is shown in Fig. 4.1. The system includes also (among various other minor components) a boost pressure pump and pressure relief valves which are not shown in the diagram. However, boost pressure pump replenishment dynamics are neglected, as in the modeling of a similar hydrostatic transmission system in [31].

Another way to conveniently represent the interrelationship of the different components is by a block diagram. A block diagram describing the relationship of the digital controller and the hydraulic system is shown in Fig. (4.2). The digital part contains A/D and D/A converters and the control algorithm and the dynamics of the physical system are described by the pump, hydraulic lines, motors, load dynamics, measurement and filtering blocks.

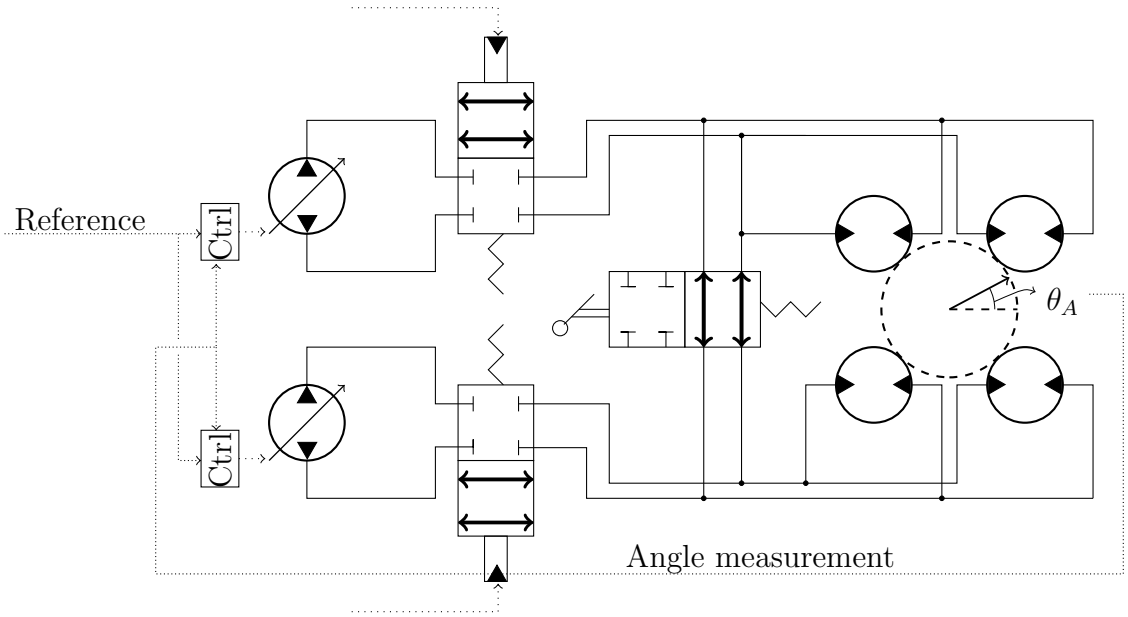

Figure 4.1: Schematic diagram of the hydraulic system.

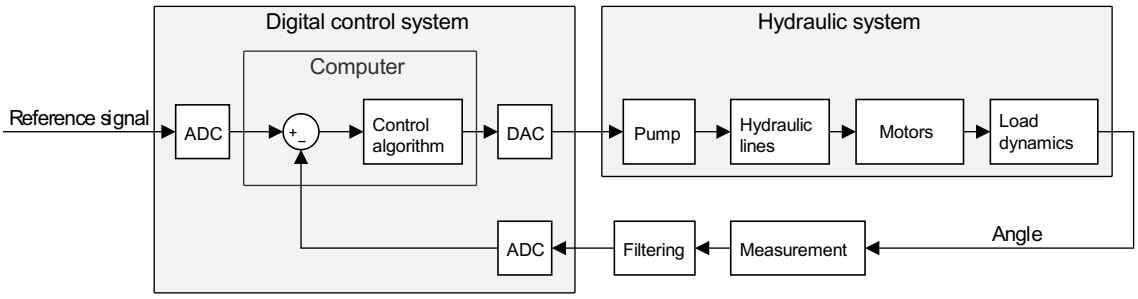

Figure 4.2: A block diagram of the computer-controlled hydraulic system.

Different valve combinations can be used to operate the system with different settings: one or two pumps with four motors or one pump with two motors. The default setting in this thesis is one pump and four motors. Using this setting the maximum steady-state angular velocity is $\dot{\theta}_A = 2.5\ ^\circ/s$. Others are examined only briefly. The maximum pump output is assumed to be $Q_p = 500$ l/min. Since using only two motors results in half of the effective motor displacement, the maximum steady-state angular velocity is doubled. The same can be achieved by using two pumps although it has a different impact on the system dynamics.

The pump output is supplied to the hydraulic lines, which consists of steel pipes and hydraulic hoses. The lengths are assumed to be $l_p = 20$ m and $l_h = 2$ m. The accumulation of hydraulic fluid in the hydraulic lines results in generation of pressure (torque in the motors). The pinions of the motors are mechanically connected to the gear ring of the load (gear ratio $R = \frac{1}{13}$) and the load responds to the torque according to the load dynamics. Since the motors and the load are mechanically linked, the rotation of the motor depends on the rotation of the load. However, a backlash exists in the connection and so the dependence is not one-to-one and the effects of backlash must be accounted for. A model describing this interaction between the hydraulic lines, the motors and the load will be developed later.

4.1.2 Variable displacement axial piston pump

Pump shaft is assumed to be rotating at a constant angular velocity regardless of the required torque. Therefore, the produced flow rate is steady and proportional to the pump's displacement. The flow rate is found from [32]

$$Q_p = \alpha_p k_p \eta_{vp} \tag{4.1}$$

where α_p is the swashplate angle, k_p is pump coefficient and η_{vp} is volumetric efficiency. Here $\alpha = \alpha_p(u_c(t), t)$ and $u_c(t)$ is the electrical control signal to the electro-hydraulic servovalve. Therefore, the pump has, from control system perspective, one input and one output, $u_c(t)$ and Q_p, respectively. The pump output flow is controlled by the swashplate angle α, which is in turn controlled by an electro-hydraulic servovalve. However, the spool dynamics of the electro-hydraulic servovalve are often significantly faster compared to the swashplate dynamics [23] and we neglect them in this thesis.

The numerical value of the swashplate angle, as measured in degrees, is unimportant. What is important is the angular velocity which the output flow creates when it flows through the motors, so for convenience we may simply define[5] that $-1 \leq \alpha_p \leq 1$ (we note that this is a linearization). The pump coefficient k_p now represents the maximum pump output.

As usual with hydraulic components, the dynamic behavior of the pump swashplate is nonlinear. Numerous authors have researched the control of axial piston pumps and the pump is often represented by a simple linear model that neglects major factors, such as load pressure and may thus be inadequate [24]. However, a linear approximation is very attractive for design purposes and we shall use that approach in this thesis. Following the approach in [23], we represent the swashplate dynamics as a critically damped second-order system (double poles). Based on the information provided by manufacturer, the minimum time required for the swashplate angle to go from zero to maximum is $T_r = 500$ ms. We take this to be the rise time ($5\% \rightarrow 95\%$), which locates the double poles at $p_p = -8.8$ rad/s. The transfer function is given by

$$G_{sp} = \frac{p_p^2}{(s - p_p)^2} = \frac{8.8^2}{s^2 - 2 \cdot 8.8s + 8.8^2}. \tag{4.2}$$

where p_p is the location of the double pole of swashplate transfer function. A step response is shown in Fig. 4.3. Contrary to this linear approximation, the swashplate angle α_p, and thus the output flow, is limited in both absolute value and in it's rate of change. Consequently, there are two types of saturations that occur in the pump which impose limitations to the use of Eq. (4.2). We assume that the maximum angular velocity is reached during a unit step response and by Eq. (4.2), the swashplate speed therefore saturates at 3.24 $1/s$.

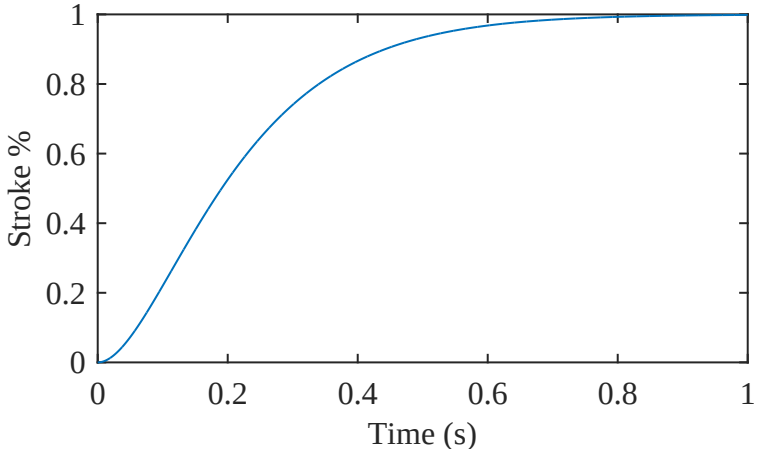

Figure 4.3: Step response of the swashplate.

[5]Similarly, we define that $-1 \leq u_c \leq 1$, which represents the desired swashplate angle.

4.1.3 Hydraulic fluid and transmission lines

Pumps and motors are connected together by hydraulic transmission lines including steel pipelines and rubber-based hoses.

The following dimensions are assumed in this thesis. The maximum lengths of the steel pipeline and hoses are 20 m and 2 m, respectively. Inner diameter of the steel pipeline is $D_i = 38\ mm$ and outer diameter is $D_o = 45.5\ mm$ and Poisson's ratio $\nu = 0.3$ and modulus of elasticity $E = 160\ GPa$ are used for steel. The inner diameter of hoses is assumed to be 25 mm for which the bulk modulus is given in [30] to be $\beta_h = 0.5\ GPa$.

Hydraulic fluid and bulk modulus. Hydraulic fluids are compressed when pressure is exerted on them and the fluid volume is decreased. The fluid volume is also altered with temperature changes, but we will assume a constant temperature in this thesis. The *(isothermal) bulk modulus* β is the ratio of change in pressure and fractional change in fluid volume in a constant temperature [19]. In practice, the same value can also be used for adiabatic compression and the change in pressure can be expressed generally as

$$\Delta P = -\beta \frac{\Delta V}{V_0} \tag{4.3}$$

where V_0 is the initial volume of the fluid and ΔV is the fluid volume change.

For petroleum fluids, the value of β is about 1.5 GPa, but it can be significantly lowered by entrained air and mechanical compliance [19]. In reality, hydraulic fluids contain also some amount of air. The volume fraction of entrained air in a hydraulic system is typically between 0.1–5 % [32] and while it is generally accepted that dissolved air has a negligible effect to bulk modulus [19, 31], entrained air in the form of bubbles can present problems [31]. Even small amounts of entrained air rapidly decrease the value of β [19] and the bulk modulus becomes a nonlinear function of pressure. Bulk modulus nonlinearities may even induce instabilities such as pressure oscillations that can cause disturbances to control systems, loss of performance and reduced component life [25]. Therefore, the effects of mechanical compliance and entrained air must be considered. Because in our model the bulk modulus affects to the pressure generation, we account for these effects by considering torque disturbances in Sec. 5.4.

Increasing the pressure in a pipe causes a radial displacement of the pipe inner surface [19] and the container volume increases (effectively decreasing the bulk modulus). To include the effects of this and those of entrained air, a parameter called *effective bulk modulus* is used. The effective bulk modulus β_e can be calculated from

$$\begin{aligned} \frac{1}{\beta_e} = \frac{1}{\beta_{la}} + \frac{V_p}{V_s}\frac{1}{\beta_p} + \frac{V_h}{V_s}\frac{1}{\beta_h} &= \frac{1}{\beta_{la}} + \frac{1}{\beta_{pipeline}} \\ \rightarrow \beta_e &= \frac{\beta_{la}\beta_{pipeline}}{\beta_{la} + \beta_{pipeline}} \end{aligned} \tag{4.4}$$

where V is volume and the subscripts la, s, p, h refer to liquid-air mixture, system, pipes (steel) and hoses respectively. For liquid-air mixtures we use the formula given in [30]

$$\beta_{la} = \beta_l \frac{1 + r_V}{1 + (\frac{P_0}{P})^{(1/\kappa)} r_V \frac{\beta_l}{\kappa P}} \tag{4.5}$$

where β_l is the bulk modulus of the liquid without entrained air, r_V is the ratio of air and liquid in the mixture, P_0 is the atmospheric pressure, P is the operating pressure and κ is the isentropic exponent ($\kappa = 1.4$). The bulk modulus for a thick-walled cylindrical container (β_p) is found from [19, 31]

$$\frac{1}{\beta_p} = \frac{2}{E} \frac{(1+\nu)D_o^2 + (1-\nu)D_i^2}{(D_o - D_i)(D_o + D_i)} \tag{4.6}$$

where E is modulus of elasticity of the container material, ν is Poisson's ratio of the container material and D_o and D_i are the outer and inner diameter, respectively, of the cylindrical container. Using the given values, we have $\beta_{pipeline} = 9.6\ GPa$. The contribution of liquid-air mixture β_{la} to effective bulk modulus is dependent on pressure and the ratio of entrained air and liquid. Fig. 4.4 shows the effective bulk modulus as a function of pressure, starting from the boost pressure 25 *bar*, with different percentages of entrained air. However, we note that these calculations provide only a rough estimate and in practice, the real effective bulk modulus is difficult to determine other than by directly measuring it [19]. Consequently, it is necessary to examine also the (static) variation of bulk modulus. This is done in Sec. 5.6.2, where the effects of parameter variations of the model are investigated.

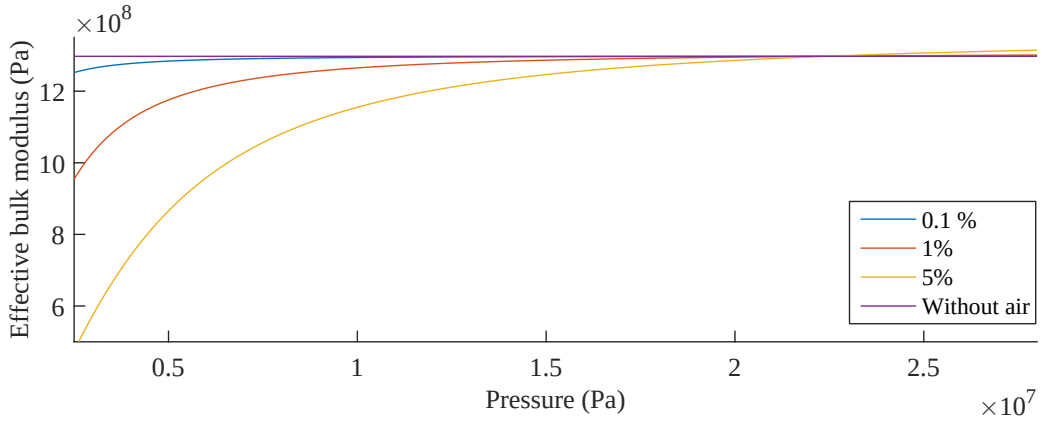

Figure 4.4: Effective bulk modulus as a function of pressure, with different percentages of entrained air.

Transmission line dynamics. The transmission lines influence the dynamics of the system. The influence increases in significance as the transmission line lengths increase [29]. These effects are caused by *hydraulic resistance* (friction), *hydraulic capacitance* (mechanical compliance and fluid compressibility) and *inertance*. The significance of these dynamic effects depends on the system and the required accuracy.

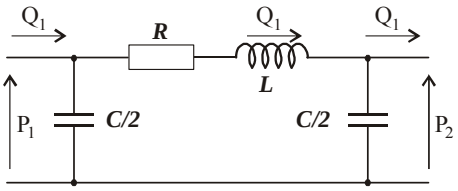

Figure 4.5: π circuit used in literature to model hydraulic transmission line dynamics. Figure taken from [28]

To produce the solution for transmission lines that satisfies the boundary conditions, fluid momentum, state and mass flow state continuity equations must be applied to an infinitesimal length of line an then integrated [31]. However, short transmission lines are commonly approximated in literature by single-lump approximations. Two such approximations are known as π and T circuits [28, 31], of which π circuit is shown in Fig. 4.5. Here R, L and C represent hydraulic resistance, inductance and capacitance, respectively.

For longer pipelines, a single-lump approximation may not describe the pipeline dynamics adequately, since it omits harmonics of higher frequencies. To obtain a proper mathematical model for such pipeline, the pipeline can be divided into multiple equal π circuits (π segments) [28, 29]. Increasing the number of π segments introduces higher frequencies to the frequency spectrum, which increases the accuracy of the model. Selection of the number of segments should be based on the frequency of the input signal and dynamics of other elements in the system. [28] However, it is suggested in [30] that for low-frequency behavior, the pipeline dynamics do not play a significant role in the input-output behavior of the system and that they can be neglected if the relationship

$$l < \frac{c}{10 f_{max}} \tag{4.7}$$

is satisfied, where l is the length of the pipeline, c is the sonic velocity in oil and f_{max} is the maximum value of the interesting frequency. Assuming that $c \approx 1400$ m/s and considering that the pump model introduced in Sec. 4.1.2 is critically damped (i.e. no transient oscillations) and has a bandwidth of only 0.9 Hz, we may conclude that only the hydraulic capacitance is of importance. In addition, the load model that will be introduced later does not exhibit significant oscillatory behavior.

A hydraulic description of pipeline capacitance, with flows and pressures, is analogous to the electrical description of capacitors with currents and voltages. Replacing currents and voltages in the mathematical equations for capacitors with flows and pressures, we have an equation for derivative of pressure with respect to time

$$\frac{dP}{dt} = \frac{Q_\Delta}{C_e} \tag{4.8}$$

where C_e is the effective hydraulic capacitance and Q_Δ is the net flow to the pipeline. The hydraulic capacitance can in turn be written as

$$C_e = \frac{V_0}{\beta_e} \tag{4.9}$$

where β_e is effective bulk modulus and V_0 is the initial volume. Therefore, the variable parameter that determines the dynamic behavior of the transmission lines is the hydraulic capacitance.

The pressure generated in the lines due to accumulated fluid is found by integrating Eq. (4.8) with respect to time, and we have

$$P(t) = P_0 + \int_{t_0}^{t} \frac{\beta_e(P)}{V_0} Q_\Delta(t) dt \tag{4.10}$$

where Q_Δ is the net influx of fluid to the transmission line and β_e is found from Eqs. (4.4) and (4.5), (plotted in Fig. 4.4). If we set $Q_\Delta = 1$ m^3/s, the integral Eq. (4.10) gives the pressure generated by unit volume. Solving this numerically, we obtain curves for pressure as a function of accumulated volume, shown in Fig. 4.6. The variation of bulk modulus with respect to pressure is more pronounced at low pressures (even more so below the boost pressure).

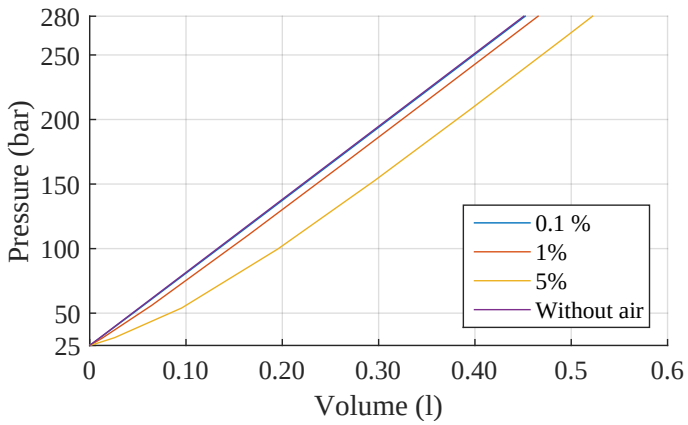

Figure 4.6: Pressure generation as a function of accumulated volume.

4.1.4 Motors

Hydraulic motors convert the pressure differential into a corresponding torque to the load, which results in a dynamic response of the load.

The four motors in the system can be reduced into one without loss of accuracy. This is because each motor is assumed to be identical with one another and to follow the same mathematical equations that determine the input-output behavior. Furthermore, the pressure inputs received by the motors are also identical, since the hydraulic transmission lines behave as volumes with hydraulic capacitance. Therefore, we simplify by reducing the motors into one with corresponding displacement and internal leakage.

The pressure differential between the input and output port of the motors is converted into torque, which is then transmitted to the load via the gearing system. Theoretically, the relationship between the motor side torque and the pressure

differential over the motor is found from [32]

$$T_m = \eta_t D_m \Delta P \tag{4.11}$$

where η_t is total efficiency, D_m is radial displacement of the motor and ΔP is pressure differential over the motor. We consider η_t to account for all mechanical losses in the system. In addition

Neglecting backlash for the moment, the relationship between the angular displacement of the motors and the load is

$$\theta_A = R\,\theta_m \tag{4.12}$$

where R is the gear ratio. Differentiating Eq. (4.12) with respect to time, we have immediately

$$\dot{\theta}_A = R\,\dot{\theta}_m, \quad \ddot{\theta}_A = R\,\ddot{\theta}_m \tag{4.13}$$

The relationship between the motor side torque and load side torque can be found by considering that the work done on the system by the motors must be absorbed by the load (and vice versa). Combining this with Eq. (4.12) results in

$$T_m\theta_m = T_A\theta_A \rightarrow T_A = \frac{1}{R}T_m. \tag{4.14}$$

where T_A is the load side torque. Combining Eqs. (4.11) and (4.14), we obtain a relationship between motor pressure differential and load side torque which can be expressed as

$$T_A = \frac{\eta_t D_m}{R}\Delta P = \eta_t D_A \Delta P \tag{4.15}$$

where $D_A = \frac{D_m}{R}$. Thus, we can see that it is the ratio of motor displacement and gear ratio that determines the torque coefficient.

Flow rates and leakages. The leakages in positive displacement pumps and motors are primarily a result of flow through small clearance spaces, called *capillary passages*, and therefore most of the internal leakage flow is laminar and can be described by the fundamental relationship of flow between flat plates [27]. Motor's internal leakage flow rates are therefore directly proportional to the pressure differential over cylinder seals and are given by the equation

$$Q_{leak} = L\Delta P_s \tag{4.16}$$

where L is leakage coefficient and ΔP_s is pressure differential over cylinder seals. Clearly there will always be leakages because of the boost pressure. However, the leakage that is the result of the boost pressure occurs at both sides and can be neglected. Therefore, we set simply $\Delta P_s = P$, where P is the absolute hydraulic motor port pressure. The total flow rate through the port of a hydraulic motor can thus be expressed as

$$Q_m = D_m\dot{\theta}_m + Q_{leak} = \frac{D_m}{R}\dot{\theta}_A + LP = D_A\dot{\theta}_A + LP \tag{4.17}$$

which describe how the motor supplies/demands hydraulic oil to/from the transmission lines.

4.1.5 Load model

The load model will be derived based on previously performed SIMULINK® modeling that is shown in Fig. 4.7. The output of the lookup table, which is shown in Fig. 4.8, represents the hydrodynamic torque applied to the load in the angle θ_A. We will consider the cases with and without the hydrodynamic torque. As can be seen, the original transfer function has three real poles (-32.7, -1.89, 0), but the order of the transfer function can be reduced by eliminating the significantly faster pole in -32.7 rad/s. This results in the following simplified transfer function

$$G_A(s) = \frac{2.5/32.7}{s(s+1.89)} \tag{4.18}$$

which we will be using in this thesis. A comparison of impulse responses between the original and simplified transfer function is shown in Fig. 4.9. The final Simulink model for the load dynamics is shown in Fig. 4.10, where K_{sc} is a coefficient used to scale the transfer function correctly with respect to the input torque[6].

Since the slope of the hydrodynamic torque is not constant throughout the operating range, the system is nonlinear and the transfer function must be defined for each linear region separately. After eliminating the feedback loop, we have

$$G_A(s) = \frac{2.5/32.7}{s(s+1.89) - 2.5/32.7 \cdot K_{hdt}} \tag{4.19}$$

where K_{hdt} is the hydrodynamic torque coefficient that assumes the values $-2.5, 0$ and 7 depending on the operating angle.

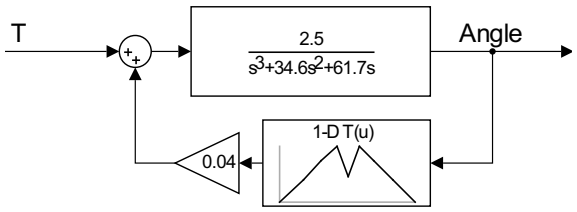

Figure 4.7: Previously used Simulink model for response to torque.

[6]We use the assumption that the static pressure differential required to maintain equilibrium at maximum hydrodynamic torque is 112.5 *bar* with four motors (with two motors the pressure differential is 225 *bar*).

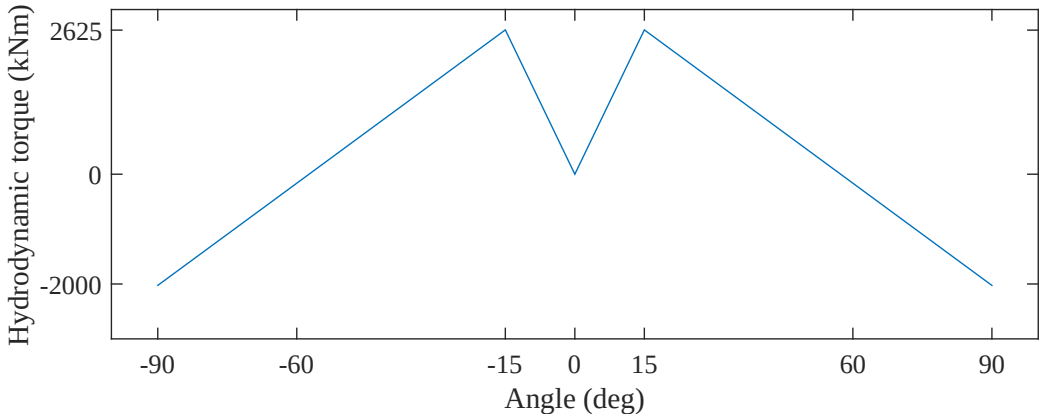

Figure 4.8: Hydrodynamic torque as a function of the angle in degrees.

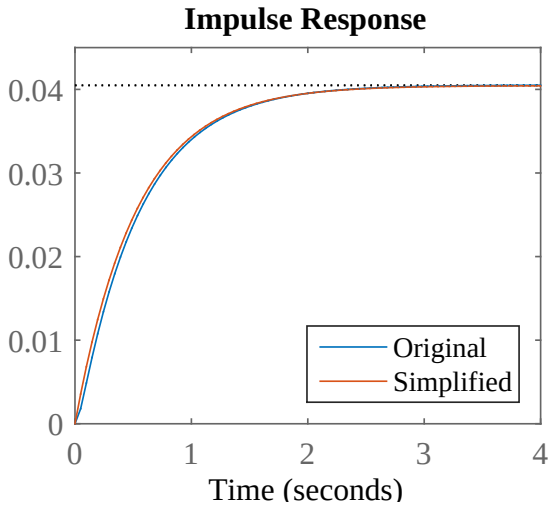

Figure 4.9: Comparison of impulse responses between the original and simplified transfer functions.

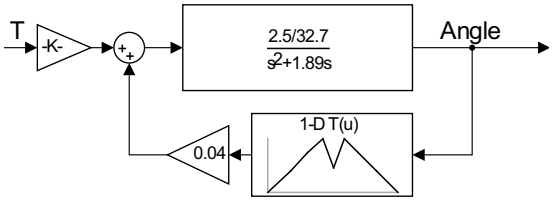

Figure 4.10: Final Simulink model for load response to torque.

4.1.6 Backlash

Backlash is the final nonlinearity in the physical system that we will consider. When the sign of the relative angular velocity between the motors and the load changes, there is a brief period during which the pinion connected to the motor is not connected to the gear ring of the load. As a result, no torque is being transmitted.

In many cases, backlash may cause inaccuracies and instability in control systems and wear out the mechanical elements [18]. In fact, multivalued nonlinearities such as backlash are often the source of discrepancies between predicted and actual results and backlash is especially notorious for causing limit cycle oscillations [19]. Therefore, it is important to investigate the effects of backlash.

Suppose that the load is stationary and that there is a contact between the pinion and the gear ring. It is given that the maximum (end-to-end) backlash measured in the load angle is $\theta_{BL} = 0.15°$. If we need to rotate the load to the other direction so

that the contact is temporarily lost, the motors will rotate freely without resistance until contact is made again. Thus, we can represent the backlash as an unrestricted flow through the motor port according to Eq. (4.17). The volume that needs to be supplied by the pump before contact is made is $\Delta V = D_A \theta_{BL}$. The behavior is thus the same as if the volume of the hydraulic line increased. Therefore, we treat backlash as a volume expansion/reduction of a hydraulic line due to the relative motion of motors and load. Assuming that a pump output $Q_p = 500 \frac{l}{min}$ generates an angular velocity $\dot{\theta}_A = 2.5\ ^\circ/s$, then $D_A = 3.33\ l/^\circ$ and $\Delta V_{BL} = 0.25\ l$.

Since at the boost pressure region, the pressure generation begins only after the line has expanded a volume of ΔV_{BL}, combining the curve in Fig. 4.6 with the line expansion, we obtain an input-output curve for pressure as a function of accumulated volume that includes the effect of backlash, as shown in Fig. 4.11. We will observe that in our model backlash actually manifests as a single-valued nonlinearity. In terms of volume accumulation and pressure, the effect is a deadband of width ΔV_{BL}. If only two motors are used, the deadband is halved. The final function is shown in Fig. 4.11.

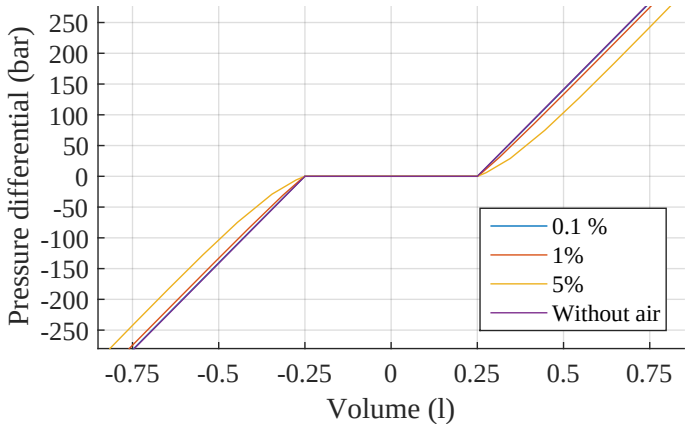

Figure 4.11: Effects of variable bulk modulus and backlash combined. Absolute pressure is obtained by adding the boost pressure of 25 bar.

4.2 SIMULINK® model

The complete model consists of two parts, the controller and the process. The Controller block contains blocks to simulate zero-order hold, the controller difference equations and quantization. The Process block consists of the hydraulic system components described in Sec. 4.1. Fig. 4.12 shows the topmost hierarchy level of the model.

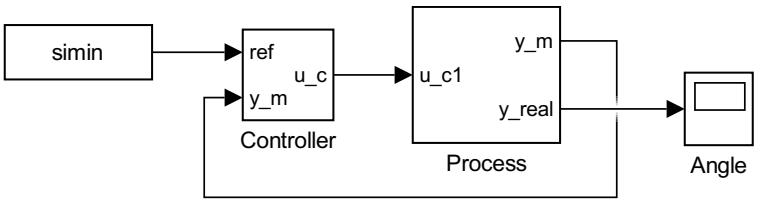

Figure 4.12: Topmost hierarchy level of the model.

Fig. 4.13 shows the contents of the Controller block. ZOH blocks represent zero-order hold with sampling period T_s. Therefore, each signal is sampled and (optionally) quantized. The quantization effects could be reduced if the sum element is placed before the quantizers (the worst-case will be reduced by one third). The block contains two controller types, of which only one is selected at a time. The reference signal *ref* and the measurement signal y_m are received as inputs and the control calculations are performed based on $ref - y_m$. The calculated control value passes through a saturation block (limits ± 1) that simulates current limitation. The final output u_c is passed on to the Process block. Processing delays are assumed to be negligible.

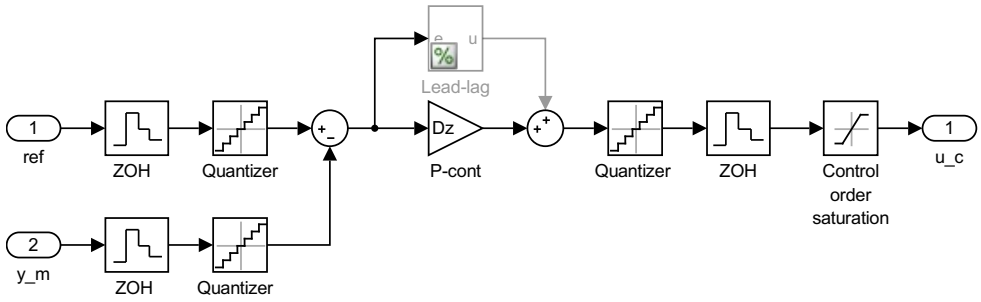

Figure 4.13: The Controller block.

The gain Dz is the gain of a simple P-controller (we refer to this value as either controller gain or the P-value) and the Lead-lag block calculates difference equations of the form

$$u[k] = Au[k-1] + B(e[k] - Ce[k-1])) \tag{4.20}$$

where $e = r - y_m$. This equation corresponds to a discrete controller

$$D(z) = B\frac{z+C}{z+A}. \tag{4.21}$$

The Process block has been divided into three sub blocks, Pump, Transmission lines and motor, and Load model as shown in Fig. 4.14 and contains also blocks to simulate the optional distortion of angle measurement; Measurement delay, Band-Limited White Noise and Low-pass filter, where fbp is the filter breakpoint. The multiplication $D_A \cdot$ deg_to_rad represents the hydraulic oil flow to the hydraulic motors corresponding to the angular velocity.

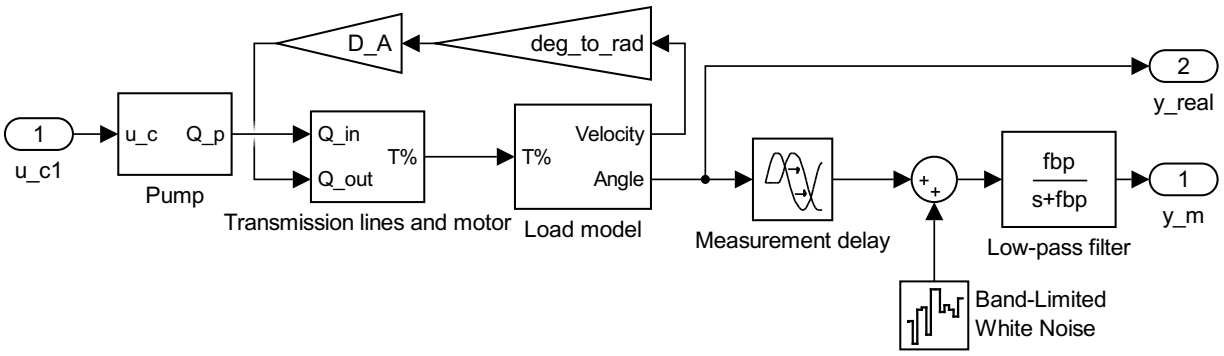

Figure 4.14: Upper hierarchy level of Process block.

The Pump block consists of the swashplate dynamics (Eq. (4.2)), angle speed limit and angle saturation. The speed is limited to $3.24\frac{1}{s}$ and angle to ± 1 according to Sec. 4.1.2. Pump coefficient is selected to be $K_p = 500\frac{l}{min}$.

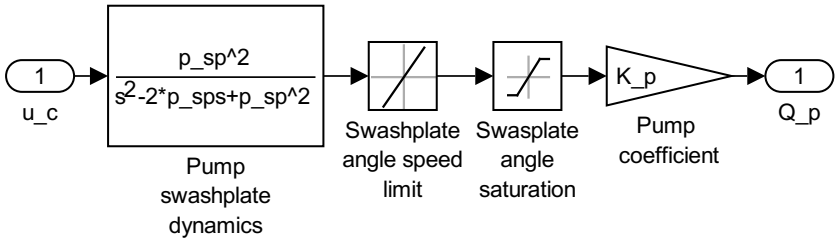

Figure 4.15: The Pump block.

The Transmission lines and motor block (Fig. 4.16) models the generation of pressure in the hydraulic motor chambers. The effect of backlash is modeled as a deadzone in terms of the accumulated hydraulic oil volume and bulk modulus

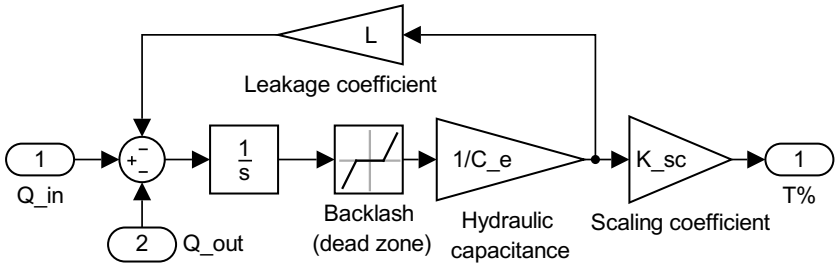

Figure 4.16: The Transmission lines and motor block.

variability is left out. The pressure differential multiplied by the leakage coefficient represents the leakage flow through the motor piston seals (see Sec. 4.1.4). If the sign of the pressure differential reverses, we assume that the low pressure line rapidly drops to boost pressure and has an insignificant effect to the dynamics. Consequently, the sign of the pressure differential indicates which one of the hydraulic lines is pressurized. A negative pressure differential results in a negative torque.

Finally, the Load model block (Fig. 4.17) simulates the dynamic behavior of the load. The values $K_{hdt} = 0$, $K_{hdt} = 7$ and $K_{hdt} = -2.5$ will be considered.

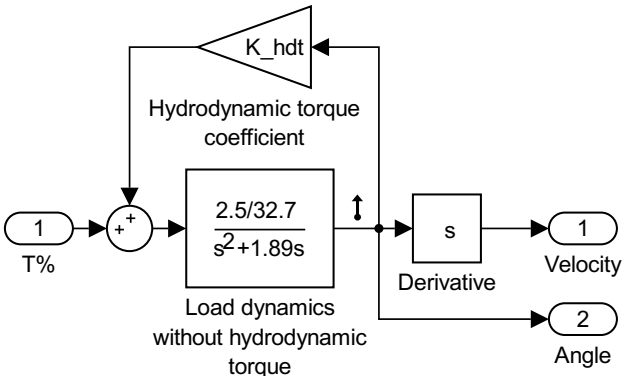

Figure 4.17: The Load model block.

4.3 Model linearization and analysis

When the nonlinearities of the foregoing model (backlash and saturations) are neglected, the dynamic behavior can be described in terms of a set of differential equations that relate the physical quantities (or the state variables) to each other. These state variables are θ_A, $\dot{\theta}_A$, α_p, $\dot{\alpha}_p$ and P (load angle, load angular velocity, pump swashplate angle and pump swashplate angular velocity and hydraulic pipeline pressure, respectively).

The derivative of pressure with respect to time is obtained from Eq. (4.8), where $Q_\Delta = \alpha_p k_p - D_A \dot{\theta}_A - LP$. Thus, the time derivative of pressure can be written as

$$\dot{P} = \frac{\beta_e}{V_0}(\alpha_p k_p - D_A \dot{\theta}_A - LP) = \frac{1}{C_e}(\alpha_p k_p - D_A \dot{\theta}_A - LP). \tag{4.22}$$

From the transfer function of swashplate in Eq. (4.2), we get the state-space representation for the pump

$$\begin{bmatrix} \dot{\alpha}_p \\ \ddot{\alpha}_p \end{bmatrix} = \begin{bmatrix} 0 & 1 \\ -p_p^2 & 2 \cdot p_p \end{bmatrix} \begin{bmatrix} \alpha_p \\ \dot{\alpha}_p \end{bmatrix} + \begin{bmatrix} 0 \\ p_p^2 \end{bmatrix} \mathbf{u_c} \tag{4.23}$$

where u_c is the control command to the pump and p_p is the double pole location describing the swashplate dynamics. Connecting transmission line equations and

load transfer function (Eq. (5.1)) we have

$$\begin{bmatrix} \dot{\theta}_A \\ \ddot{\theta}_A \\ \dot{P} \end{bmatrix} = \begin{bmatrix} 0 & 1 & 0 \\ K_A K_{hdt} & -1.89 & K_A K_{sc} \\ 0 & -D_A/C_e & -L/C_e \end{bmatrix} \begin{bmatrix} \theta_A \\ \dot{\theta}_A \\ P \end{bmatrix} + \begin{bmatrix} 0 \\ 0 \\ 1/C_e \end{bmatrix} K_p \alpha_p \tag{4.24}$$

where $K_p\alpha_p$ is the pump output flow, K_A is the numerator of the load model and K_{sc} is the scaling factor between the transmission lines and load model. When we group the two state-space equations in Eqs. (4.23) and (4.24) into a single state-space representation, we arrive at the final state-space representation

$$\begin{bmatrix} \dot{\theta}_A \\ \ddot{\theta}_A \\ \dot{P} \\ \dot{\alpha}_p \\ \ddot{\alpha}_p \end{bmatrix} = \begin{bmatrix} 0 & 1 & 0 & 0 & 0 \\ K_A K_{hdt} & -1.89 & K_A K_{sc} & 0 & 0 \\ 0 & -D_A/C_e & -L/C_e & K_p/C_e & 0 \\ 0 & 0 & 0 & 0 & 1 \\ 0 & 0 & 0 & -p_p^2 & 2p_p \end{bmatrix} \begin{bmatrix} \theta_A \\ \dot{\theta}_A \\ P \\ \alpha_p \\ \dot{\alpha}_p \end{bmatrix} + \begin{bmatrix} 0 \\ 0 \\ 0 \\ 0 \\ p_p^2 \end{bmatrix} \mathbf{u_c} \tag{4.25}$$

This state-space representation describes the linearized process dynamics and can be used to investigate the poles of the system. If antialiasing filtering is included, we have to include also one additional state for the measured signal. We will use the simplest low-pass filter introduced in Eq. (2.18). The differential equation is

$$\dot{\theta}_f(t) = \omega_f(-\theta_f(t) + \theta_A(t)). \tag{4.26}$$

After adding this state, we have

$$\begin{bmatrix} \dot{\theta}_A \\ \ddot{\theta}_A \\ \dot{P} \\ \dot{\alpha}_p \\ \ddot{\alpha}_p \\ \dot{\theta}_f \end{bmatrix} = \begin{bmatrix} 0 & 1 & 0 & 0 & 0 & 0 \\ K_A K_{hdt} & -1.89 & K_A K_{sc} & 0 & 0 & 0 \\ 0 & -D_A/C_e & -L/C_e & K_p/C_e & 0 & 0 \\ 0 & 0 & 0 & 0 & 1 & 0 \\ 0 & 0 & 0 & -p_p^2 & 2p_p & 0 \\ \omega_f & 0 & 0 & 0 & 0 & -\omega_f \end{bmatrix} \begin{bmatrix} \theta_A \\ \dot{\theta}_A \\ P \\ \alpha_p \\ \dot{\alpha}_p \\ \theta_f \end{bmatrix} + \begin{bmatrix} 0 \\ 0 \\ 0 \\ 0 \\ p_p^2 \\ 0 \end{bmatrix} \mathbf{u_c}. \tag{4.27}$$

or

$$\dot{\mathbf{x}} = \mathbf{A}\mathbf{x} + \mathbf{B}\mathbf{u_c} \tag{4.28}$$

Using matrix notation, we can represent negative feedback control by setting

$$\mathbf{u_c} = -\mathbf{K}\mathbf{x} \tag{4.29}$$

where $\mathbf{K}$ is the control law. The closed-loop system will then be described by

$$\dot{\mathbf{x}} = (\mathbf{A} - \mathbf{B}\mathbf{K})\mathbf{x} + \mathbf{B}\mathbf{r} \tag{4.30}$$

where $\mathbf{r}$ is the reference signal.

For robustness yet good step response characteristics we select $\mathbf{K} = \begin{bmatrix} 0.53 & 0 & 0 & 0 & 0 & 0 \end{bmatrix}$ for the continuous-time controller. The step response of this configuration is shown in Fig. 4.18. This continuous-time controller will be used

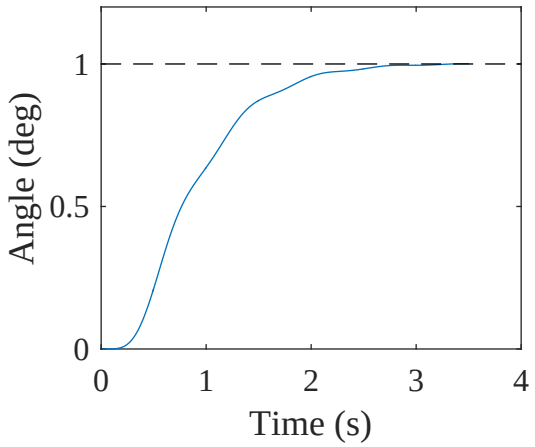

Figure 4.18: Step response of the linearized continuous system.

as a reference for the digital controller. Note that the sixth state remains unused in the continuous-time system, which means that antialiasing filtering will not be included.

This configuration leads to a closed-loop bandwidth of $w_b = 2.03$ rad/s $= 0.32$ Hz, which according to the discussion of sample rate selection in Sec. 2.2 suggests that the sample rate should be selected somewhere between 3 to 13 Hz. We will be investigating sample rates between 5 to 20 Hz in this thesis.

The controllability matrices are full rank in both cases and therefore the five (six) pole locations of this system can be arbitrarily selected by an appropriate full state control law (see pole location analysis in Sec. 3.4). While this is not possible when using a P-controller based on angle measurement, the discrete plant model obtained from discretization of Eq. (4.27) yields the exact system states under ideal conditions (i.e. perfect plant model and no nonlinearities). These estimated states can then be used instead of the actual values. For detailed discussion of estimators and estimator design (Kalman filter in particular), the reader is advised to read [2, 3]. However, the step response in Fig. 4.18 suggests that a simple P-controller is sufficient. Since our goal is to find the simplest controller that results in equivalent performance, we will focus on control based on measured angle alone.

According to the developed nonlinear model, the obtained linearized transfer function is identical to the nonlinear model provided that

1. Controller output does not exceed 1 and thus saturate the control order, i.e. $|u_c(t)| \leq 1$
2. Controller output does not cause swashplate speed to exceed it's maximum, i.e. $|\dot{\alpha}| \leq 3.24/s$
3. One of the hydraulic lines is pressurized (no backlash effects)
4. Quantization effects are ignored

In most cases that we will be studying, the conditions 1 and 2 can be considered to be fulfilled and the effects of quantization and measurement noise can be superposed to

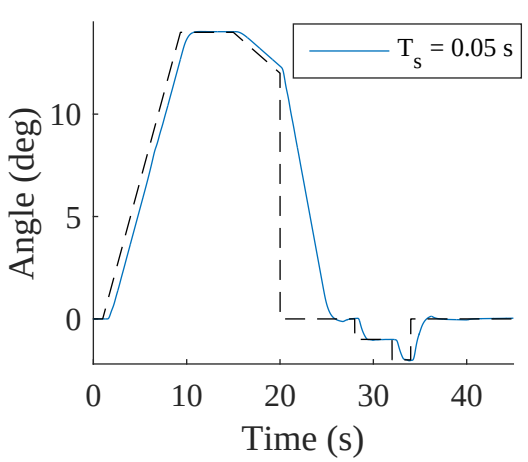

Figure 4.19: Response of the nonlinear model.

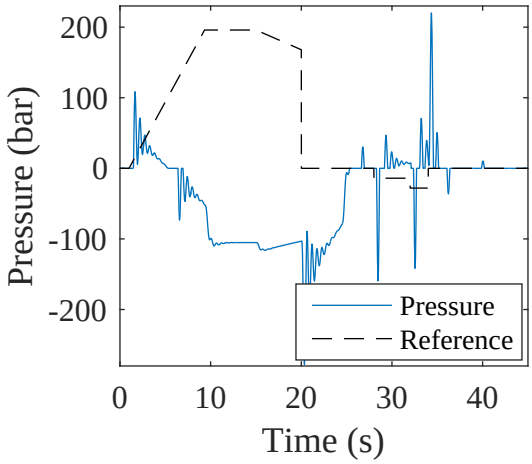

Figure 4.20: Pressure of the nonlinear model as a function of time.

the linear response. Furthermore, the condition 3 is fulfilled most of the time when hydrodynamic torque $K_{hdt} = 7$ and $|\theta_A| \geq 1°$. This is readily seen from Figs. 4.19 and 4.20, which shows that the lines are indeed pressurized most of the time when $|\theta_A| \geq 1°$. However, near the angle $\theta_A \approx 0°$, backlash requires special attention due to potential limit cycles. The combined effects of quantization and backlash must be considered.

The developed linear model enables us to investigate the factors that contribute to the behavior of the system. For now, we assume default parameter values and antialiasing filter breakpoint $f_{fbp} = 2$ Hz. Since the feedback is based on the filtered measurements, only the last column of the control law is used. We select control laws that result in very similar step responses

$$\mathbf{K_{0.05s}} = \begin{bmatrix} 0 & 0 & 0 & 0 & 0 & 0.46 \end{bmatrix}$$

$$\mathbf{K_{0.10s}} = \begin{bmatrix} 0 & 0 & 0 & 0 & 0 & 0.43 \end{bmatrix}$$

$$\mathbf{K_{0.20s}} = \begin{bmatrix} 0 & 0 & 0 & 0 & 0 & 0.38 \end{bmatrix}.$$

The discretization of Eq. (4.25) that gives the discrete-time model of the system is performed in MATLAB® by invoking the **c2d.m** function with zero-order hold option. Discretizing Eq. (4.27), switching to transfer function representation and taking the partial fraction expansion (see Sec. 3.3) yields the following transfer

functions for each sampling period

$$H_{0.05s}(z) = \frac{0.00775z - 0.0170}{z^2 - 1.56z + 0.87} + \frac{-0.0174z + 0.0323}{z^2 - 1.78z + 0.80} + \frac{0.0100z - 0.0060}{z^2 - 1.052z + 0.282}$$

$$H_{0.10s}(z) = \frac{0.0023z - 0.0314}{z^2 - 0.689z + 0.753} + \frac{-0.0114z + 0.0600}{z^2 - 1.607 + 0.6551} + \frac{0.0097z - 0.0040}{z^2 - 0.53z + 0.08}$$

$$H_{0.20s}(z) = \frac{-0.0252z - 0.0380}{z^2 + 1.06z + 0.5871} + \frac{0.0357z + 0.0987}{z^2 - 1.335z + 0.4662} + \frac{0.0017z - 0.0011}{z^2 - 0.0966 + 0.0054}. \tag{4.31}$$

As we see, each transfer function (sixth-order system) consists of a sum of three second-order transfer functions. The poles of each term are also poles of the sixth-order system. Superposition principle tells us that the final response can be found by adding the responses of the terms, e.g. $H(z)U(z) = \big[H_1(z) + H_2(z) + \cdots + H_n(z)\big]U(z)$, where $H(z)$ describes the system and $U(z)$ is the input. This enables us to examine the contributions of the different components and how they are affected when parameters are varied.

A plot of system poles using z-plane to s-plane mapping ($z = e^{sT}$) is perhaps more informative. The poles of the different systems are shown in Fig. 4.21. These poles represent either critically damped poles (only real roots) or damped oscillations (see z-plane to s-plane mapping in Sec. 3.4). Each of the (discrete) pole pairs are the poles of the transfer functions in Eq. (4.31). All of the systems have two oscillatory poles (leftmost terms) of relatively low damping (for $T_s = 0.20$ s the oscillations are aliased to a lower frequency) and four oscillatory poles of high damping. Plotting the step responses for each term individually (Figs. 4.22 and 4.23), we see that when assuming default values the second term (the pole pair in the middle) virtually determines the response. The second and third terms are of a low magnitude and have only very small effect to the system.

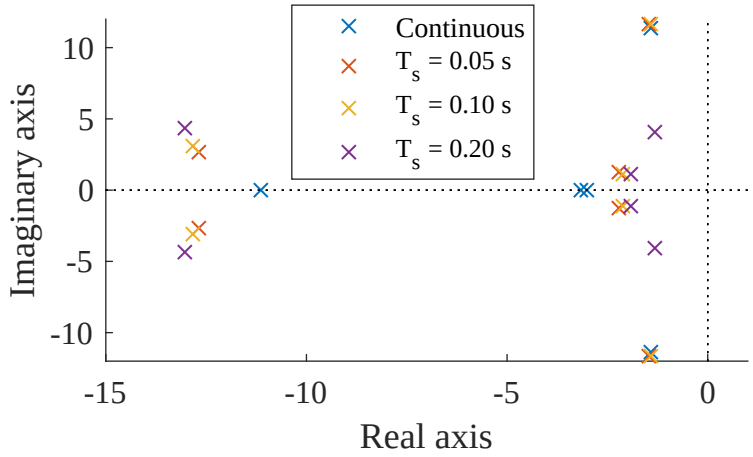

Figure 4.21: Poles of the continuous-time and discrete-time systems.

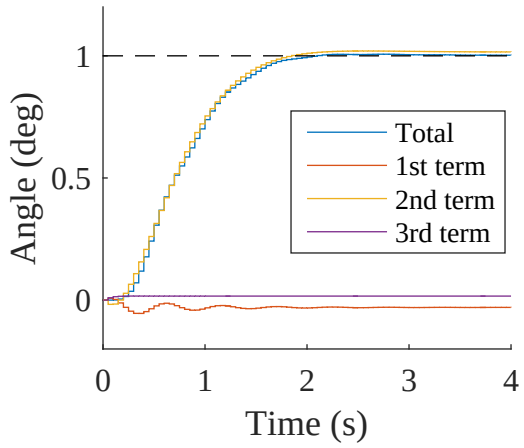

Figure 4.22: $T_s = 0.05$ s. Contributions of the terms to the total response.

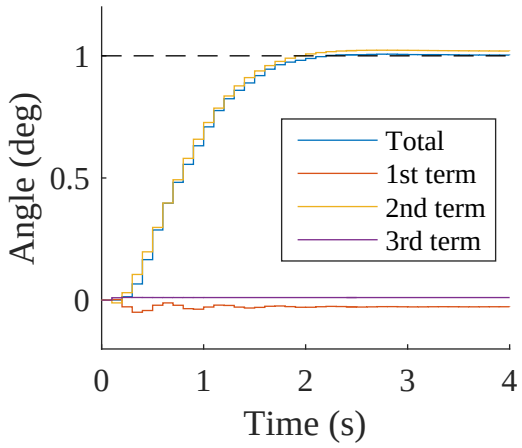

Figure 4.23: $T_s = 0.10$ s. Contributions of the terms to the total response.

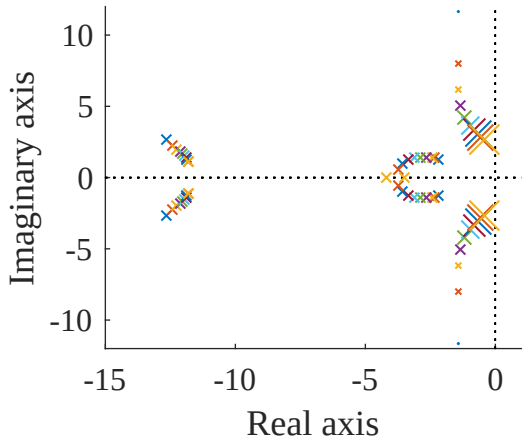

Figure 4.24: $T_s = 0.05$ s. Pole locations and variation of hydraulic capacitance from factor of 1 to 10. For middle poles, pole movement is from right to left .

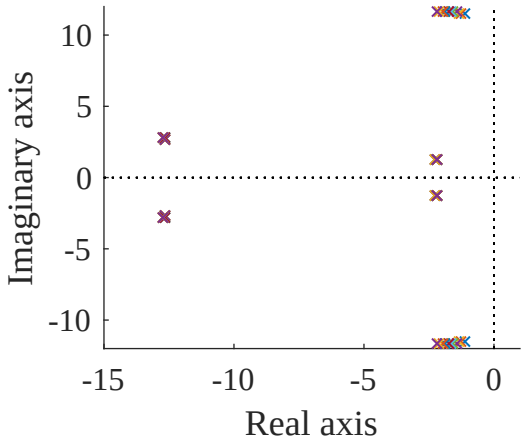

Figure 4.25: $T_s = 0.05$ s. Pole locations and variation of leakage coefficient from 0 to 40 l/min. For rightmost poles, pole movement is from right to left.

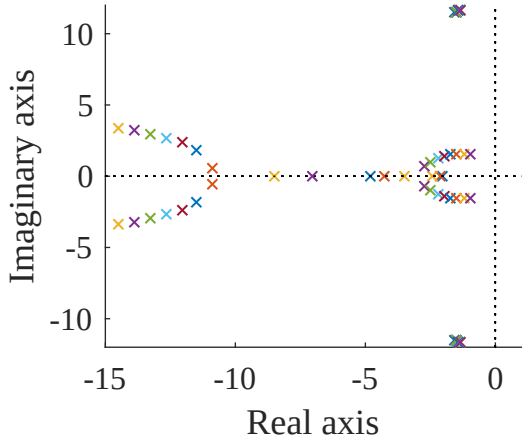

Figure 4.26: $T_s = 0.05$ s. Pole locations and variation of pump double pole location from +50% to -50% (faster to slower). Pole movement is from left to right.

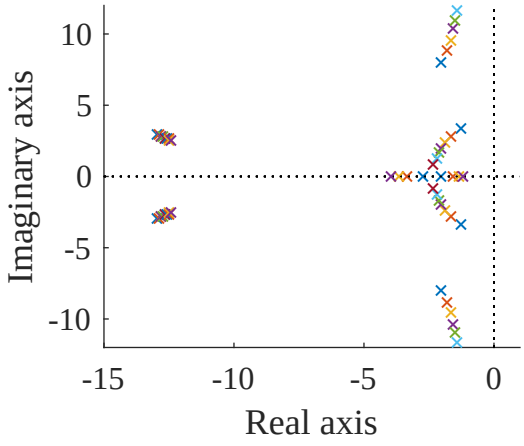

Figure 4.27: $T_s = 0.05$ s. Pole locations and variation of motor displacement from -50% to +50%. Oscillation frequency decreases and damping increases.

To examine how different parameters influence the system, we vary the parameters and plot the corresponding pole locations. Fig. 4.24 shows the pole locations as the hydraulic capacitance is increased, where the rightmost poles are plotted in proportion to the oscillation amplitude. As can be seen, the oscillation amplitude increases with hydraulic capacitance.

Increasing the leakage coefficient has a very isolated effect. All it does is to increase the damping of the oscillatory poles. There is almost no effect to the other poles.

Considering the variation of pump double pole location p_p and that the leftmost terms are much faster than the other poles (the dynamic effects can be neglected), we see that the effect of pump dynamics has also an isolated effect and mainly influences to the damping of the system.

As an ending to this section, we illustrate the power of full state feedback in a digital control system and the limitations of a P-controller. Although the pole placement approach will not be utilized in the results section since it is not considered necessary, this is nevertheless an interesting comparison.

For the purposes of this illustration, we increase the hydraulic capacitance by a factor of 7 and compare the responses obtained by a continuous P-controller and a digital controller ($T_s = 0.05$ s) with full state feedback. From Fig. 4.24 we expect that, if no modifications are made to the controller, the oscillations in the response will increase significantly due to increased magnitudes of the oscillatory poles. However, we can restore the original pole locations (see Fig. 4.21) exactly by using Ackermann's formula (**acker.m** in MATLAB®) and pole placement. This yields the control law

$$\mathbf{K} = \begin{bmatrix} 0.2626 & 0.5647 & 0.0351 & 2.0959 & 0.0421 & 3.0982 \end{bmatrix}, \tag{4.32}$$

which restores the original pole locations.

The responses are presented in Fig. 4.28. The response of the digital controller is practically the same as with the default hydraulic capacitance. This is not surprising since the two systems have the exact same pole locations. However, it has to be remembered that not all control laws are physically realizable due to saturations (although in this case the responses were simulated with saturations included). Contrary to the digital controller, no matter how the P-value is chosen for the continuous controller, the original response cannot be restored. Increasing the P-value decreases rise time but also increases oscillations.

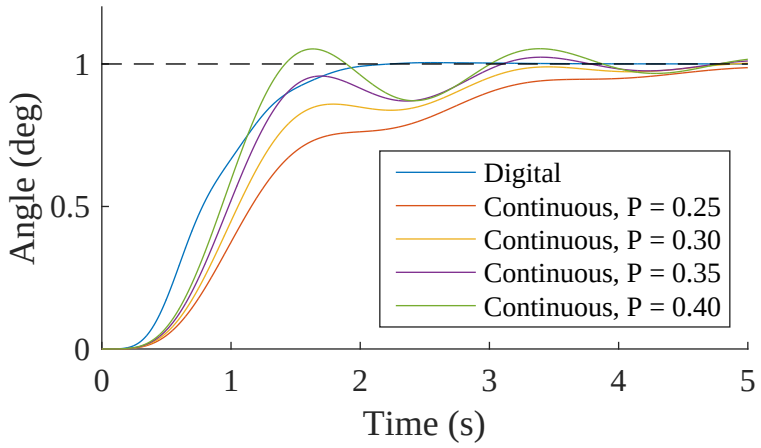

Figure 4.28: Step responses of a digital controller with restored poles and a continuous P-controller with different P-values. Hydraulic capacitance was increased by a factor of 7.

5 Results

In this section, testing results of the model developed in Sec. 4 are presented. In order to avoid excessive number of simulations and different combinations, certain design decisions are made as this section proceeds, which are then assumed throughout the rest of the simulations. Based on the discussion on sample rate selection in Sec. 2.2 and the closed-loop bandwidth of the system (Sec. 4.3), we will focus on three sampling periods $T_s = 0.05$ s, $T_s = 0.10$ s and $T_s = 0.20$ s. One of the most important goals of this section is to show the differences and similarities between the digital and analog controllers. The reasoning being that if two controllers lead to very similar responses and in various conditions, then as long as there will not be any excessive deviations between the model and reality, the performance of the controllers should not be radically different from each other even if there were effects that were not modeled.

First, we consider the linear case (i.e. no quantization, backlash or saturations) and the effects of measurement delays, antialiasing filtering, measurement noise and external disturbances. Since nonlinearities are neglected and the system is linear, the effects can be scaled. Second, we consider the effects of quantization and backlash. Finally, the performances of the discrete controllers are compared to the continuous controller under model parameters variations. The main goal is not to study the sensitivity (although it is implied by the results) but rather to determine whether there exists discrete controllers that will result in a similar performance as the continuous controller.

Unless specified otherwise, the following default values are assumed throughout this section: Pump output $K_p = 0.0833\frac{m^3}{s} = 500\frac{l}{min}$, pump swashplate double pole location $p_p = -8.8$ rad/s, hydraulic oil flow through motors per radian (load) $D_A = 0.191\frac{m^3}{rad}$ (i.e. the ratio of motor displacement and gear ratio), hydraulic capacitance $C_e = 1.77 \cdot 10^{-11}\ \frac{Pa}{m^3}$, hydrodynamic torque coefficient $K_{hdt} = 7$ and leakage coefficient $L = 1.11 \cdot 10^{-11}\frac{m^3/s}{Pa}$ (15 l/min).

Throughout the results section we will examine the performance differences between the continuous controller and the digital controller. For this purpose, a realistic reference signal, shown in Fig. 5.1, is used at times. From now this reference signal shall be called the *test signal*.

5.1 Step response with nominal parameter values

A natural starting point is to consider the step responses of the default system, i.e. no measurement delays, filtering, noise or disturbances. Under these conditions, a simple P-controller results satisfactory responses for each sampling period. The responses are shown in Fig. 5.2. In order to maximize the similarity of the responses, controller gains were selected as follows:

$$T_s = 0.05 \text{ s} \rightarrow P = 0.51$$
$$T_s = 0.10 \text{ s} \rightarrow P = 0.49$$
$$T_s = 0.20 \text{ s} \rightarrow P = 0.46$$

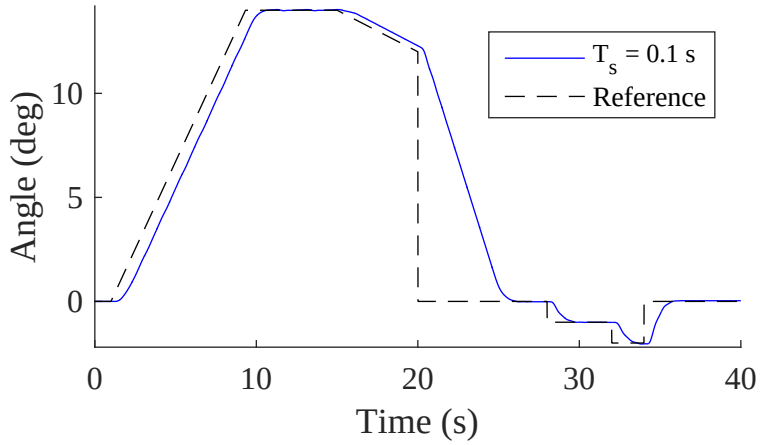

Figure 5.1: Test signal used throughout the results section. Response with a discrete controller with sampling period $T_s = 0.10\ s$ is shown as an example.

Thus, as the sampling period was increased, the controller gain had to be reduced in order to maintain the shape of the response.

Although we will not focus on more extreme sampling periods, we note that increasing the sampling period would necessitate reducing the controller gains even further ($T_s = 0.40\ s \rightarrow P = 0.4, T_s = 0.5\ s \rightarrow P = 0.37$). Fig. 5.3 shows the step responses. The P-values were again adjusted to better correspond to the continuous response.

5.2 Measurement delays and antialiasing filtering

In this section we will study the effects of antialiasing filtering and measurement delays on the dynamic behavior of the system. We will then attempt to find a controller that restores the original step response characteristics and again maximizes the similarity between the continuous (undelayed) response. From Sec. 2.3 we expect that antialiasing filtering and measurement delays will have similar effects, which

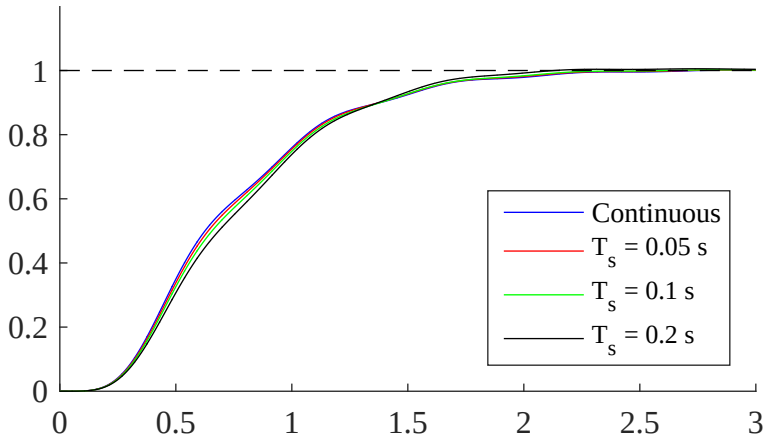

Figure 5.2: Linear step responses with different sampling periods.

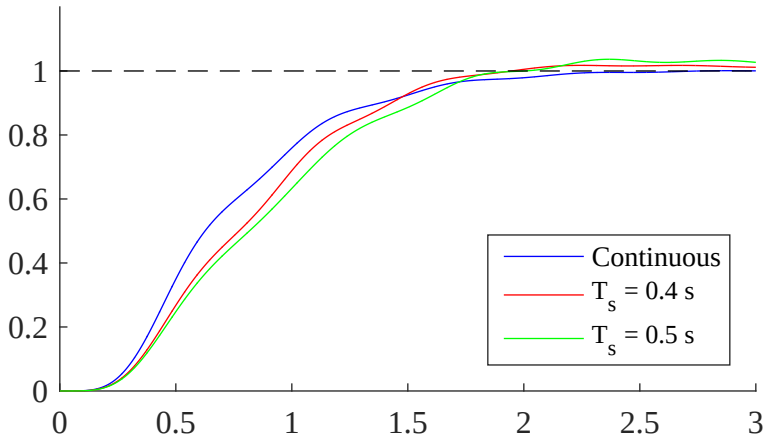

Figure 5.3: Linear step responses with more extreme sampling periods.

would suggest that one could be used to approximate the existence of another.

The upper limit for measurement delays was set to $T_{dm} = 0.20$ s and the lower limit for antialiasing filter breakpoint to $f_{fbp} = 2$ Hz. The justification for this breakpoint will be provided in the next subsection, Sec. 5.3, concerned with measurement noise.

Case 1: Uncompensated delays.
To gain insight to the dynamic effects of delays, changes in the step responses were examined as the measurement delays were increased and the controllers remained unchanged. In addition to the plots, the overshoots were tabulated.

Figs. 5.4 – 5.6 show the step responses for uncompensated delays with the sampling periods of interest. Table 5.2 shows the corresponding overshoot percentages.

Case 2: Uncompensated filtering.
Next, filter breakpoints were sought for the first-order antialiasing filter that would approximately correspond to the delays considered previously. To do this, the overshoots were matched.

Figs. 5.7 – 5.9 shows that measurement delays and filtering had indeed very similar effects. The corresponding delays were plotted, for reference, to the figures as well. In terms of step response behavior, measurement delays mapped very closely to filter breakpoints as follows:

$$T_{dm} = 0.05 \text{ s} \rightarrow f_{fbp} = 3.3 \text{ Hz}$$
$$T_{dm} = 0.10 \text{ s} \rightarrow f_{fbp} = 1.7 \text{ Hz}$$
$$T_{dm} = 0.20 \text{ s} \rightarrow f_{fbp} = 0.8 \text{ Hz}.$$

Case 3: Combined effects with and without controller changes.
As a final case, the conservative case with maximum measurement delay of $T_{dm} = 0.20$ s and a low antialiasing filter breakpoint $f_{fbp} = 2$ Hz was considered.

The step responses were similar for all sampling periods in both cases, although a slight increase in phase lag (with previous controllers) is discernible as the sam-

pling period is increased. However, to achieve the shown step responses, different controllers had to be used. The used controllers were

$$D_{0.05}(z) = 1.5(1 - 0.73z^{-1}), D_{0.10}(z) = 1 - 0.62z^{-1}, D_{0.20}(z) = 0.6 - 0.4z^{-1}. \quad (5.1)$$

Because z^{-1} means a delay of one sampling period, these controllers can be thought to include a velocity approximation, $(e[k] - e[k-1])/T_s$.

The Figs. 5.11-5.13 show that with appropriate controller changes, the responses are practically equivalent.

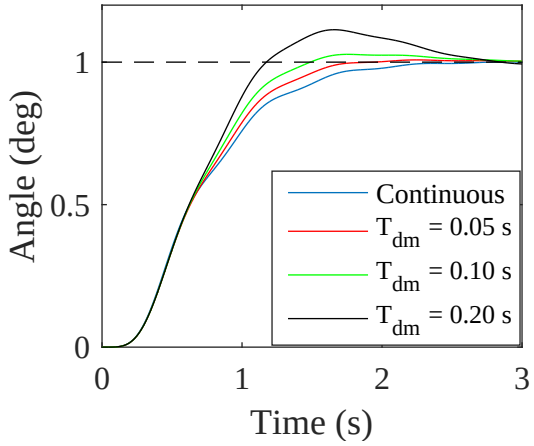

Figure 5.4: Uncompensated delays, $T_s = 0.05$ s.

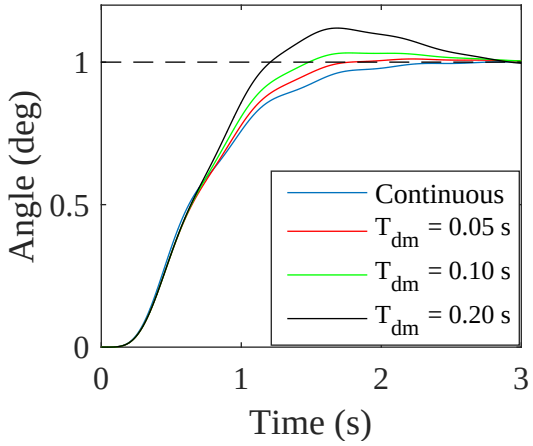

Figure 5.5: Uncompensated delays, $T_s = 0.10$ s.

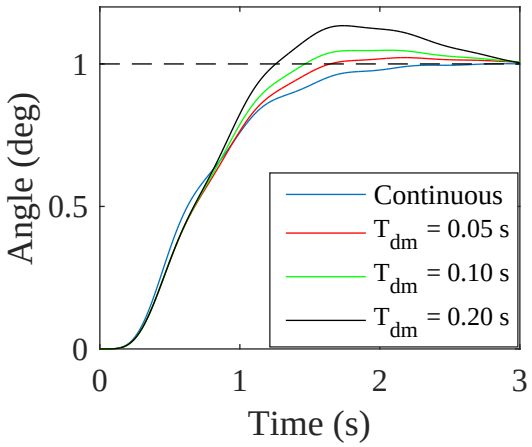

Figure 5.6: Uncompensated delays, $T_s = 0.20$ s.

T_s	T_{dm} 0.05 s	T_{dm} 0.10 s	T_{dm} 0.20 s
0.05 s	0.8%	2.7%	11.4%
0.10 s	1.1%	3.2%	11.9%
0.20 s	2.2%	4.8%	13.4%

Table 5.1: Uncompensated delays, percent overshoots.

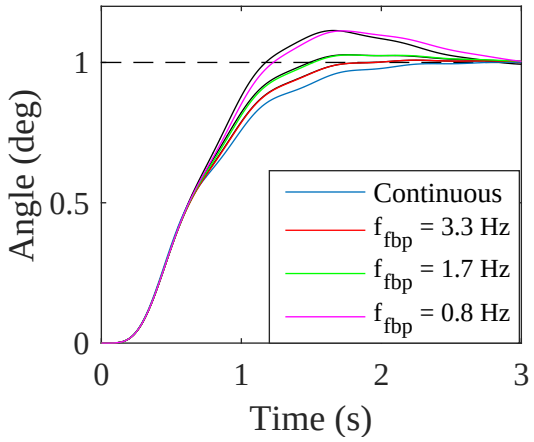

Figure 5.7: Uncompensated filtering, $T_s = 0.05$ s. Black lines in the background are the delays considered previously.

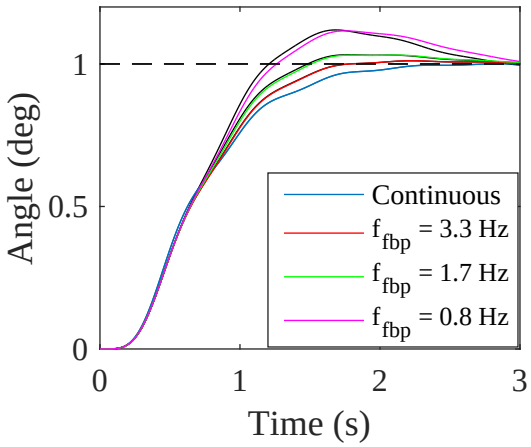

Figure 5.8: Uncompensated filtering, $T_s = 0.10$ s. Black lines in the background are the delays considered previously.

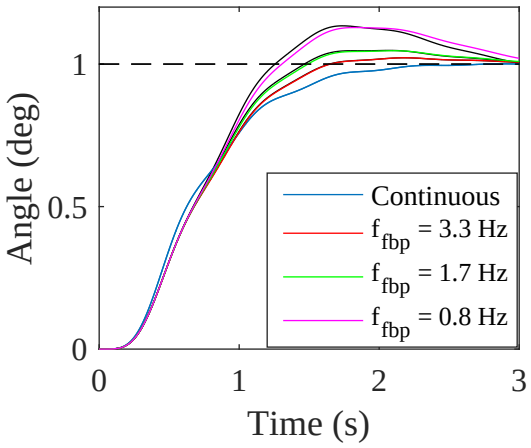

Figure 5.9: Uncompensated filtering, $T_s = 0.20$ s. Black lines in the background are the delays considered previously.

T_s	T_{dm} 0.05 s	T_{dm} 0.10 s	T_{dm} 0.20 s
0.05 s	0.8%	2.7%	11.3%
0.10 s	1.1%	3.1%	11.6%
0.20 s	2.2%	4.7%	12.8%

Table 5.2: Uncompensated filtering, percent overshoots.

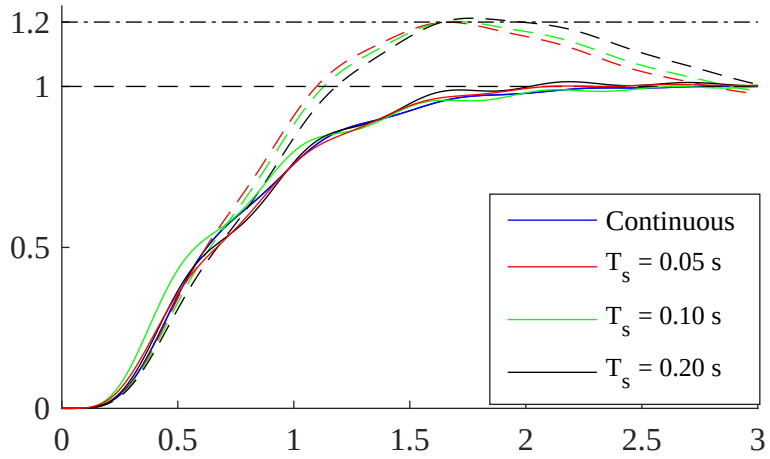

Figure 5.10: Combined effects of filtering and measurement delay. $f_{fbp} = 2$ Hz and $T_{dm} = 0.20$ s. Solid lines are the responses for improved controllers and dashed lines represent the responses with the original controllers.

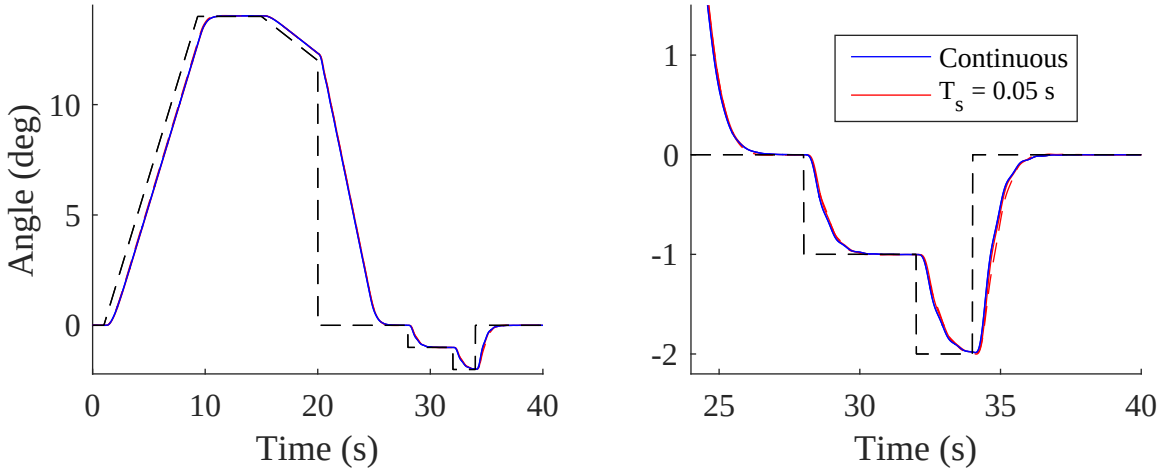

Figure 5.11: Response to test signal. Filtering and measurement delays with improved controllers, $T_s = 0.05$ s. $f_{fbp} = 2$ Hz and $T_{dm} = 0$ s $\rightarrow$ solid red line. 2 Hz filtering and $T_{dm} = 0.20$ s $\rightarrow$ dashed red line.

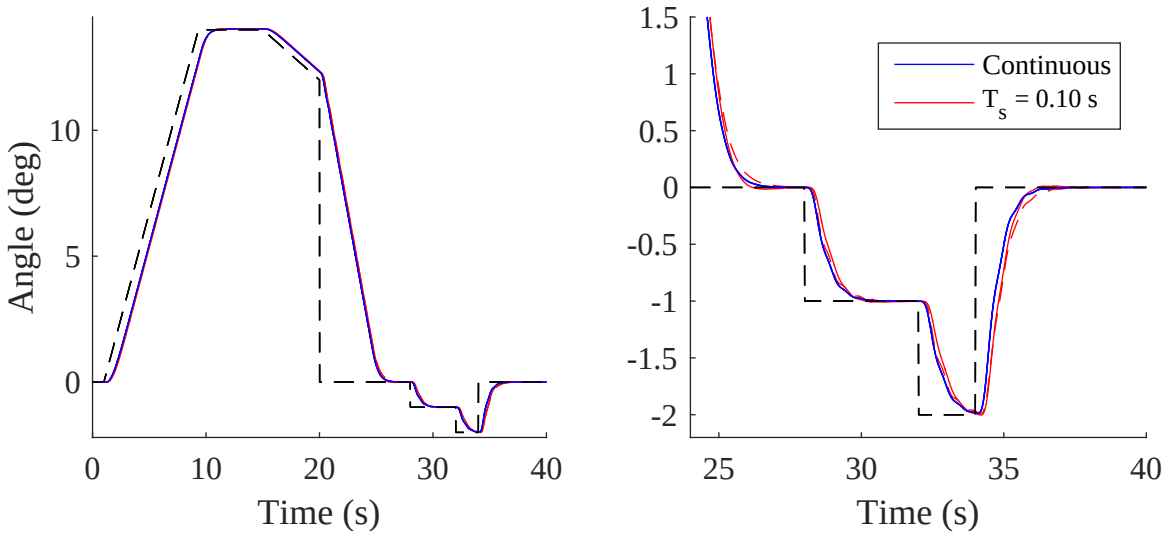

Figure 5.12: Response to test signal. Filtering and measurement delays with improved controllers,
$T_s = 0.10$ s. $f_{fbp} = 2$ Hz and $T_{dm} = 0$ s $\rightarrow$ solid red line. 2 Hz filtering and $T_{dm} = 0.20$ s $\rightarrow$ dashed red line.

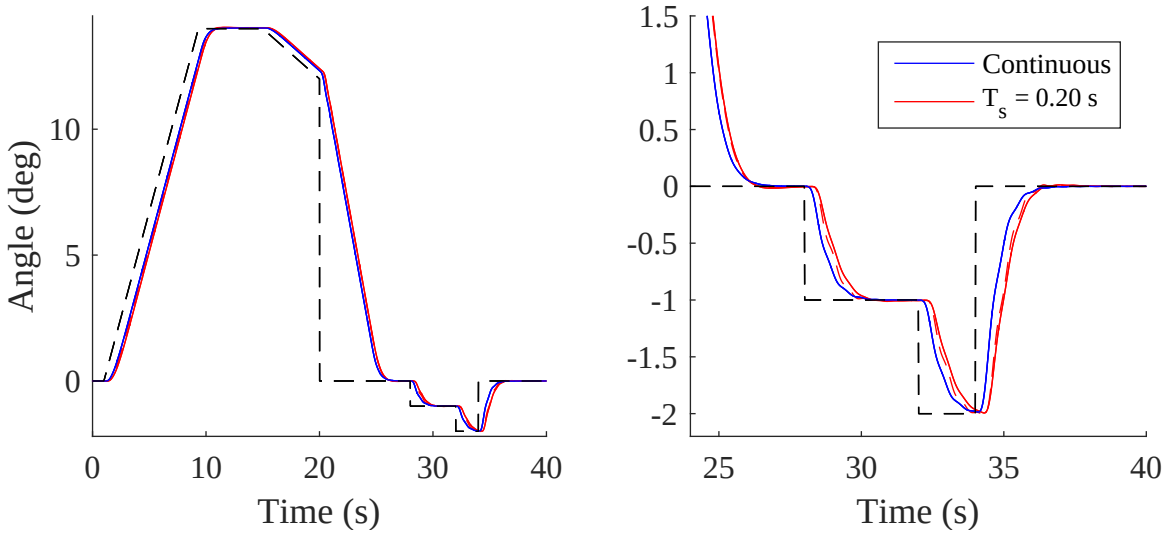

Figure 5.13: Response to test signal. Filtering and measurement delays with improved controllers,
$T_s = 0.20$ s. $f_{fbp} = 2$ Hz and $T_{dm} = 0$ s $\rightarrow$ solid red line. 2 Hz filtering and $T_{dm} = 0.20$ s $\rightarrow$ dashed red line.

5.3 Measurement noise

The effects of measurement noise were considered for multiple antialiasing filter breakpoints f_{fbp}. Mean absolute amplitude, standard deviation and maximum deviation of the responses were observed (however, contrary to the shown responses, the simulation time was 40 s and reference $r(t) = 0$). If linearity is assumed, these results are scaleable with respect to the mean absolute amplitude of the noise. However, if the amplitude is increased significantly, saturations must be considered. For comparison, the measurement noise response of the continuous system is shown in Fig. 5.14.

The type of noise considered was bandlimited white noise, entering the system as shown in Fig. 4.14. Noise power was set to 0.016, so that the mean absolute amplitude of the noise was 1°.

As we showed previously, the dynamic behavior of the system is dependent on the antialiasing filter breakpoint. Therefore, the controllers were modified to approximately match the step response of the continuous system. The controllers used for each T_s and f_{fbp} are shown next to the figures. If $f_{fbp} \geq 6$ Hz, the effect to the dynamic behavior will be small and we will therefore select it as the highest filter breakpoint frequency. Unfiltered responses were not considered since filtering is necessary in a digital control system.

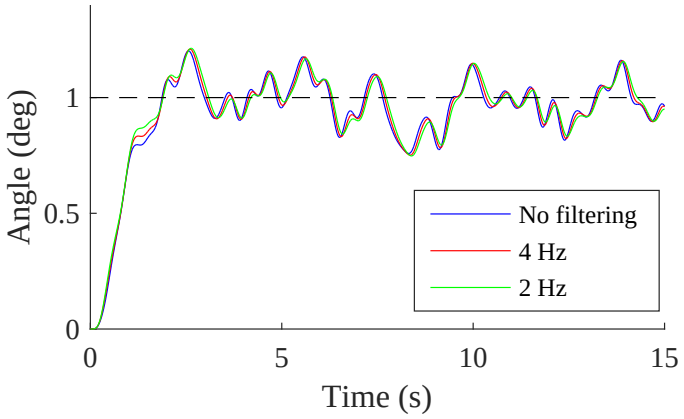

Figure 5.14: Noise response, continuous system.

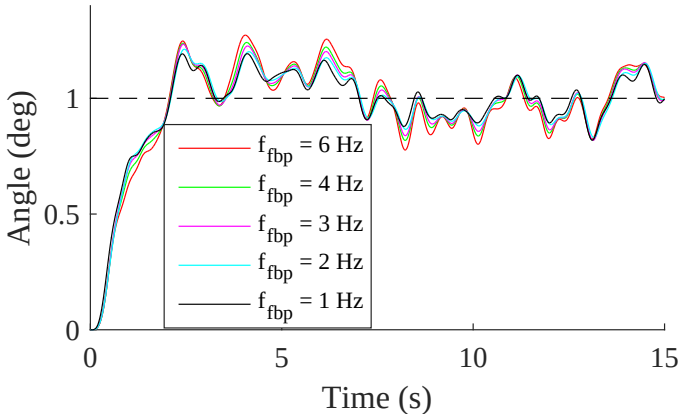

f_{fbp}	Control
6 Hz	0.48
4 Hz	0.48
3 Hz	0.48
2 Hz	0.46
1 Hz	1.5-0.7 z^{-1}

Figure 5.15: Noise response, $T_s = 0.05$ s.

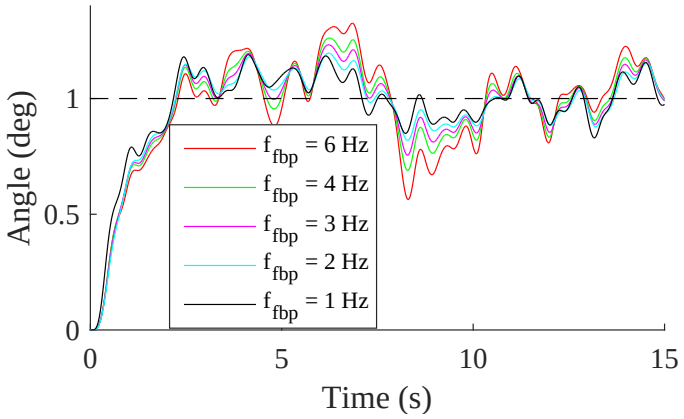

f_{fbp}	Control
6 Hz	0.46
4 Hz	0.46
3 Hz	0.45
2 Hz	0.43
1 Hz	1.0-0.57 z^{-1}

Figure 5.16: Noise response, $T_s = 0.10$ s.

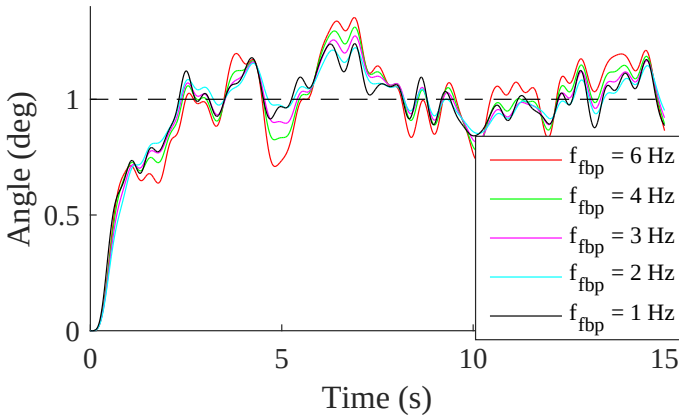

f_{fbp}	Control
6 Hz	0.43
4 Hz	0.42
3 Hz	0.40
2 Hz	0.38
1 Hz	0.6-0.35 z^{-1}

Figure 5.17: Noise response, $T_s = 0.20$ s.

f_{fbp}	Mean abs	SD	Max
6 Hz	0.09	0.12	0.33
4 Hz	0.09	0.11	0.31
3 Hz	0.09	0.10	0.30
2 Hz	0.08	0.10	0.28
1 Hz	0.08	0.09	0.26

Table 5.3: Measurement noise statistics, $T_s = 0.05$ s.

f_{fbp}	Mean abs	SD	Max
6 Hz	0.12	0.15	0.44
4 Hz	0.10	0.12	0.32
3 Hz	0.09	0.11	0.31
2 Hz	0.09	0.10	0.27
1 Hz	0.08	0.09	0.28

Table 5.4: Measurement noise statistics, $T_s = 0.10$ s.

f_{fbp}	Mean abs	SD	Max
6 Hz	0.16	0.20	0.46
4 Hz	0.13	0.15	0.38
3 Hz	0.11	0.13	0.34
2 Hz	0.09	0.10	0.30
1 Hz	0.08	0.09	0.28

Table 5.5: Measurement noise statistics, $T_s = 0.20$ s.

f_{fbp}	Mean abs	SD	Max
No filt.	0.09	0.11	0.37
4 Hz	0.09	0.11	0.36
2 Hz	0.09	0.11	0.35

Table 5.6: Measurement noise statistics, continuous.

5.4 Disturbances

The effects of two types of disturbances were examined, namely step-like disturbances and bandlimited white noise disturbances. In both cases the disturbance was inserted as an additional torque to the load model (see input no. 1 in Fig. 4.17).

For white noise disturbance, the noise power was set to $1.4 \cdot 10^{10}$ (corresponding to 10 bar mean absolute pressure). For step like disturbances, the disturbance magnitude was set to equal the torque that results from a 10 bar pressure differential. The step disturbance alternated between -10 bar and 10 bar, switching every 1 second. The selection of this time period was due to the fact that it was found to result in the most oscillatory behavior.

Antialiasing filter with a breakpoint of $f_{fbp} = 2$ Hz was also included and controller gains were adjusted as previously.

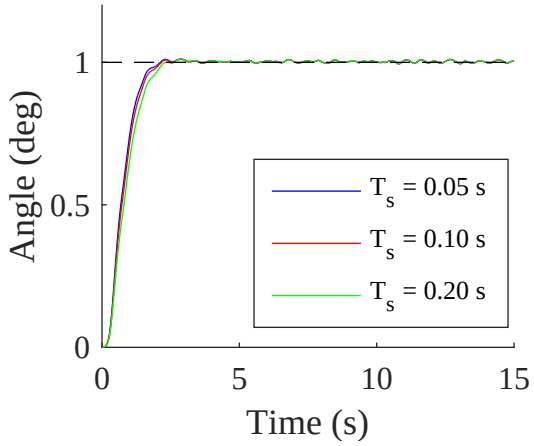

Figure 5.18: Bandlimited white noise disturbance.

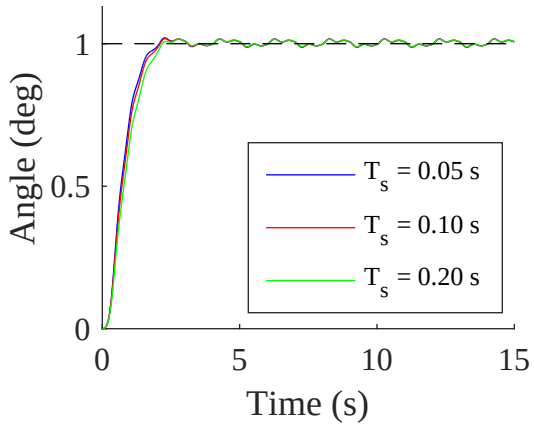

Figure 5.19: Step-like disturbance.

5.5 Nonlinearities

From now on we will include both quantization and backlash in our simulations unless stated otherwise. First, we will investigate the effects of quantization. Second, the effects of backlash will be considered. Antialiasing filtering with a breakpoint of 2 Hz was again included.

5.5.1 Quantization

Word sizes of 10-bit, 12-bit and 16-bit were studied and the difference between the quantized system output and nonquantized system output was observed. For this purpose, the test signal (Fig. 5.1) was used.

The Figs. 5.20–5.22 show the difference as a function of time. Statistics of these figures (mean absolute deviation, standard deviation and maximum absolute deviation) are shown in Tables 5.7–5.9.

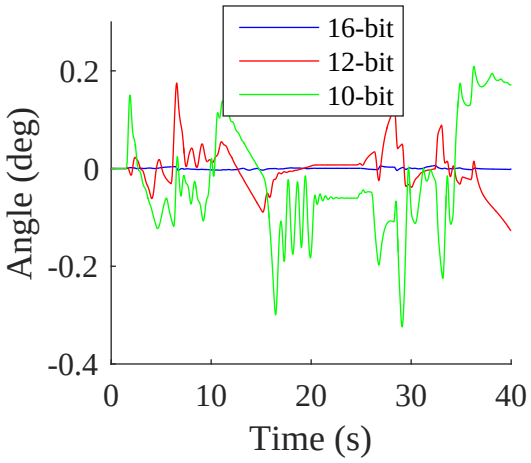

Figure 5.20: Deviation, $T_s = 0.05$ s.

$T_s = 0.05$ s

Bits	Abs mean	SD	Max
16	0.00	0.00	0.01
12	0.03	0.04	0.18
10	0.10	0.11	0.32

Table 5.7: Statistics of Fig. 5.20.

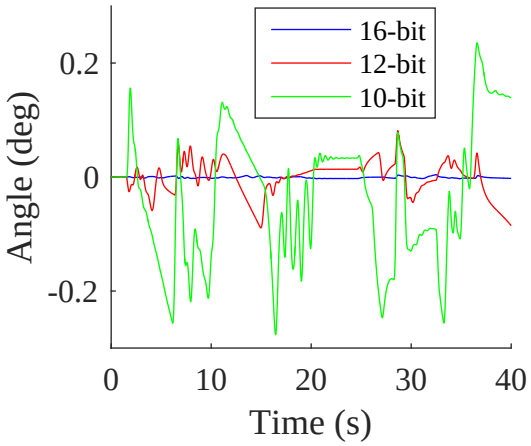

Figure 5.21: Deviation, $T_s = 0.10$ s.

$T_s = 0.10$ s

Bits	Abs mean	SD	Max
16	0.00	0.00	0.00
12	0.02	0.03	0.09
10	0.10	0.11	0.28

Table 5.8: Statistics of Fig. 5.21.

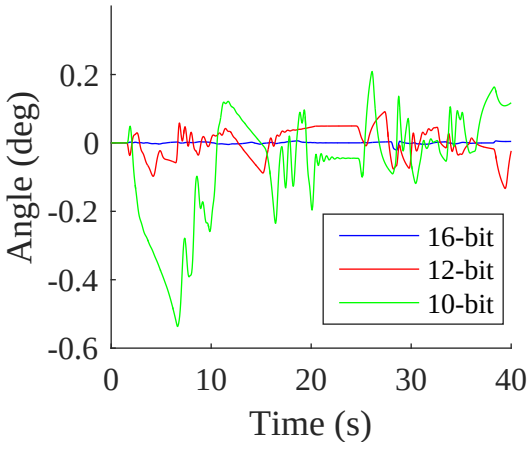

Figure 5.22: Deviation, $T_s = 0.20$ s.

$T_s = 0.20$ s

Bits	Abs mean	SD	Max
16	0.00	0.00	0.02
12	0.04	0.04	0.13
10	0.11	0.15	0.54

Table 5.9: Statistics of Fig. 5.22.

5.5.2 Backlash (deadband)

The purpose of this section was to study the existence and nature of limit cycles and the contributing factors. Two cases were examined for each sampling period, namely with and without external disturbances. It was considered that applying a random disturbance would provide a convenient way of testing the effects of backlash.

To isolate the effects of quantization from the possible effects caused by zero-order hold, a continuous-time controller with amplitude quantization was included for reference. It was assumed that the most unstable case would be when hydrodynamic torque $K_{hdt} = 7$ and was the only case studied.

First, the existence of limit cycles was explored without external disturbances by varying the controller gains. The goal was to find regions of controller gains where limit cycles did or didn't exist. Second, external disturbances were applied to see whether they could induce limit cycles or cause significant unwanted effects when combined with backlash. A white noise type of torque disturbance was already shown not to have any significant effects without backlash. The type of disturbance used was the same as in Sec. 5.4), namely bandlimited white noise, except that the mean absolute amplitude was increased to equivalent of 15 bar pressure to produce more distinguishable effects.

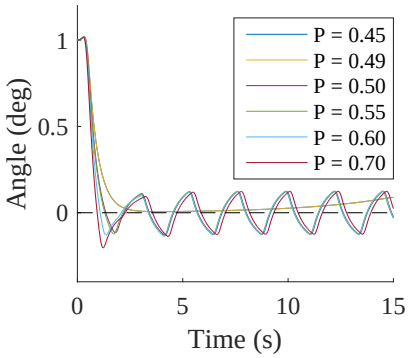

Figure 5.23: Continuous, 12-bit, no disturbances.

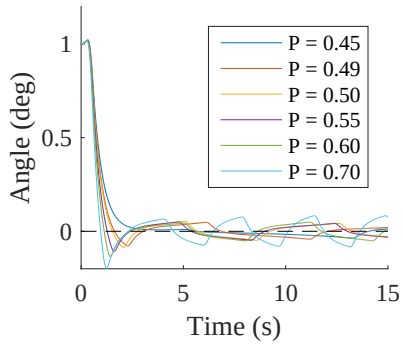

Figure 5.24: Continuous, 16-bit, no disturbances.

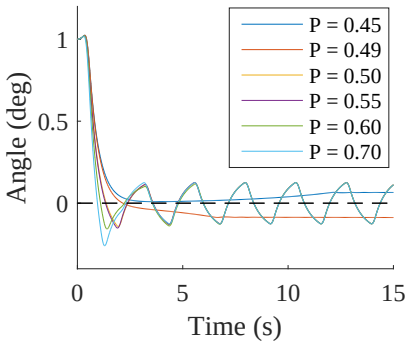

Figure 5.25: $T_s = 0.05$ s, 12-bit, no disturbances.

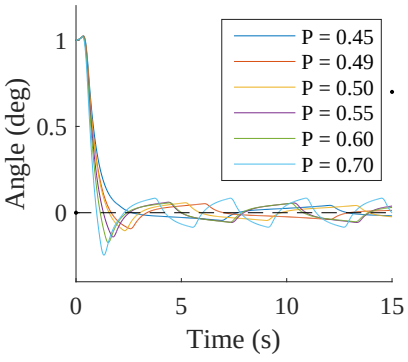

Figure 5.26: $T_s = 0.05$ s, 16-bit, no disturbances.

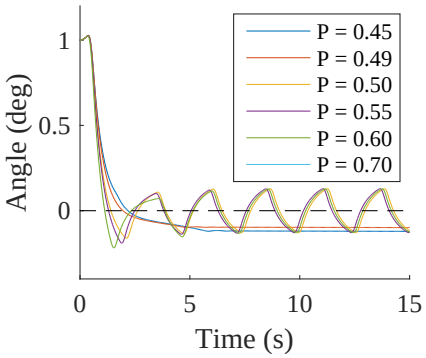

Figure 5.27: $T_s = 0.10$ s, 12-bit, no disturbances.

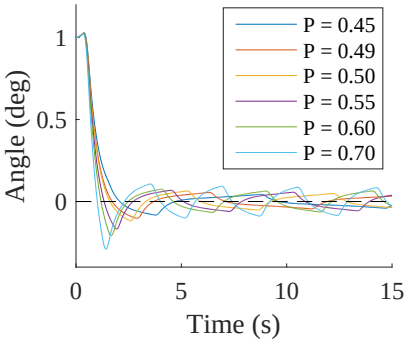

Figure 5.28: $T_s = 0.10$ s, 16-bit, no disturbances.

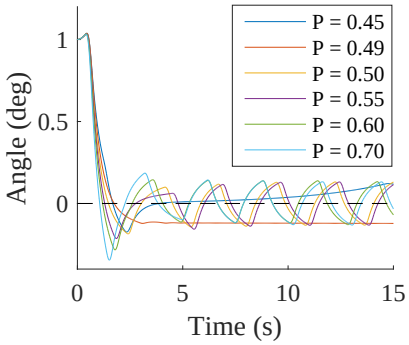

Figure 5.29: $T_s = 0.20$ s, 12-bit, no disturbances.

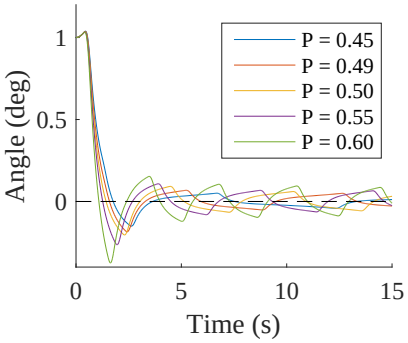

Figure 5.30: $T_s = 0.20$ s, 16-bit, no disturbances.

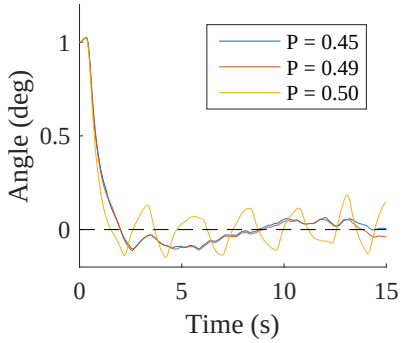

Figure 5.31: Continuous, 12-bit, disturbances included.

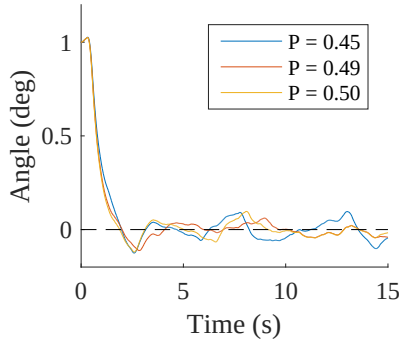

Figure 5.32: Continuous, 16-bit, disturbances included.

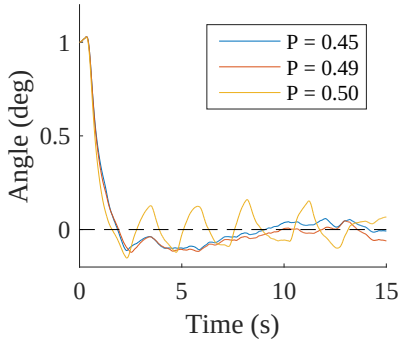

Figure 5.33: $T_s = 0.05$ s, 12-bit, disturbances included.

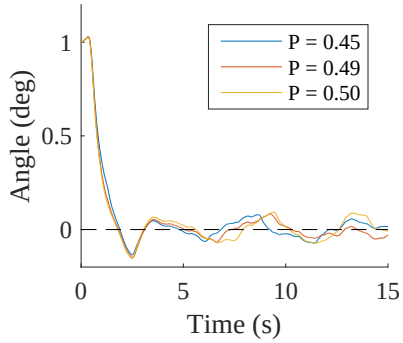

Figure 5.34: $T_s = 0.05$ s, 16-bit, disturbances included.

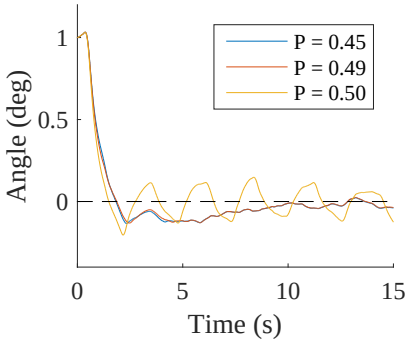

Figure 5.35: $T_s = 0.10$ s, 12-bit, disturbances included.

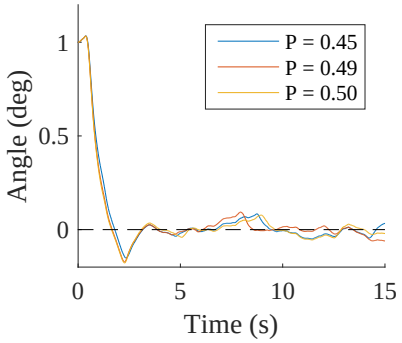

Figure 5.36: $T_s = 0.10$ s, 16-bit, disturbances included.

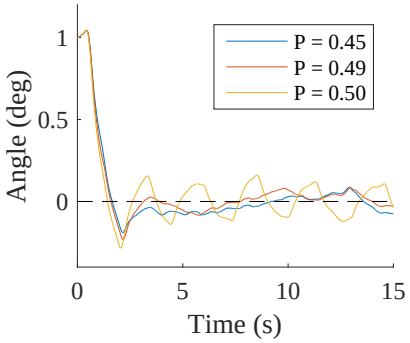

Figure 5.37: $T_s = 0.20$ s, 12-bit, disturbances included.

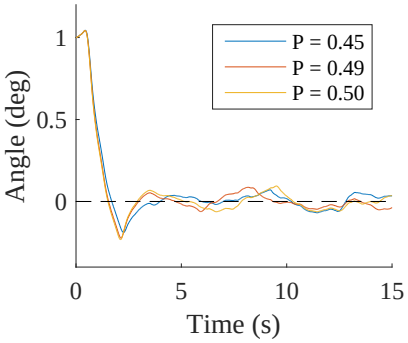

Figure 5.38: $T_s = 0.20$ s, 16-bit, disturbances included.

5.6 Model parameter variations

Finally, we turn to investigate the effects of parameter variations. In practice the parameters of the model will not be fixed and a certain amount of variation must be allowed. Despite the parameter variations, the digital control system performance must not be significantly degraded with respect to the continuous control system.

In order to reduce the number of simulations, only one parameter was varied at a time while rest of the parameters assumed default values that were given in the beginning of the results section. Possible cross effects were not considered.

Unless specified otherwise, 12-bit word size was used for quantization and as previously, anti-aliasing filter ($f_{fbp} = 2$ Hz) was included for dynamic effects. In most cases the controllers had to be modified.

5.6.1 Hydrodynamic torque

Three different hydrodynamic torque coefficients were investigated. They were $K_{hdt} = 7$, $K_{hdt} = 0$ and $K_{hdt} = -2.5$. To illustrate the influence of hydrodynamic torque alone, quantization or backlash were not included and the controllers were not modified.

The step responses are presented in Fig. 5.39. The figure shows three plots for each sampling period. For each sampling period, the curves are nearly identical

and no attempt was made to distinguish between them. This suggests that hydrodynamic torque has very little influence except possibly when combined with backlash. The effects for $K_{hdt} = 7$ together with backlash were already considered in Sec. 5.5.2.

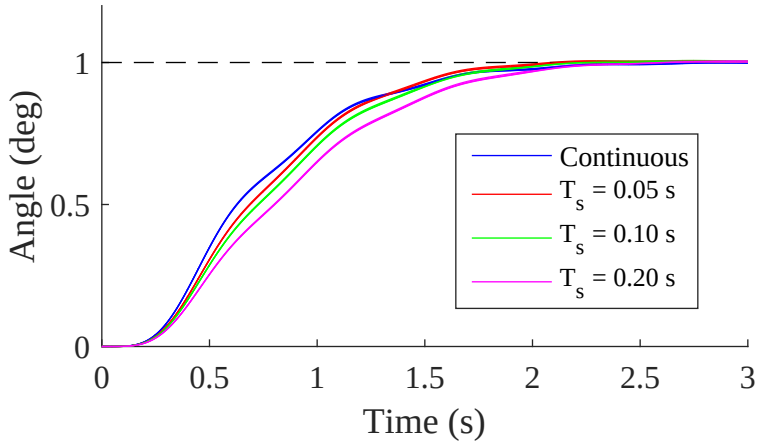

Figure 5.39: Step responses with hydrodynamic torque coefficients $K_{hdt} = 7$, $K_{hdt} = 0$ and $K_{hdt} = -2.5$,.

5.6.2 Hydraulic capacitance

Determination of effective bulk modulus is usually very difficult without direct measurements. Therefore, the effects of changing the hydraulic capacitance, C_e, were examined. This encompasses both the variation in bulk modulus and the variation in hydraulic transmission line lengths. We investigated two cases, multiplication by factors of 2 and 10, that is $C_e = 2 \cdot 1.767 \cdot 10^{-11}$ and $C_e = 1.767 \cdot 10^{-10}$. The pole location analysis in Sec. 4.3 showed that the effect of increasing hydraulic capacitance is to lower the oscillation frequency and increase it's amplitude. Therefore, the dynamic performance is expected to degrade as the hydraulic capacitance is increased.

New controller gains were selected based on the step responses (Figs. 5.40 and 5.41). For double capacitance the controllers were

$$\begin{aligned} T_s = 0.05 \text{ s} &\rightarrow P = 0.41 \\ T_s = 0.10 \text{ s} &\rightarrow P = 0.38 \\ T_s = 0.20 \text{ s} &\rightarrow P = 0.35 \end{aligned}$$

For tenfold capacitance, the controllers were

$$\begin{aligned} T_s = 0.05 \text{ s} &\rightarrow D(z) = 0.5(1 - z^{-1}) \\ T_s = 0.10 \text{ s} &\rightarrow D(z) = 0.5(1 - z^{-1}) \\ T_s = 0.20 \text{ s} &\rightarrow D(z) = 0.6(1 - 0.9z^{-1}) \end{aligned}$$

Coincidentally, the sampling periods $T_s = 0.10$ s and $T_s = 0.20$ s resulted in almost identical step responses when capacitance was doubled. They are not distinguishable from the plot.

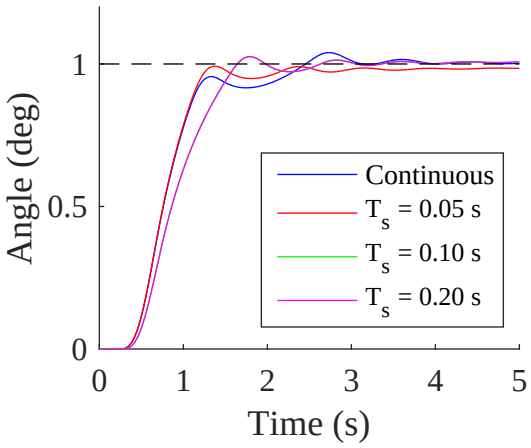

Figure 5.40: Step response, double capacitance.

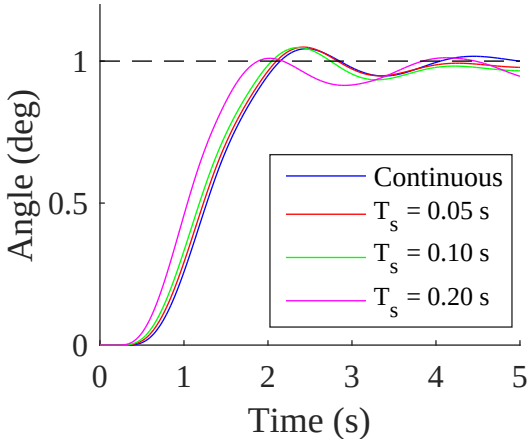

Figure 5.41: Step response, tenfold capacitance.

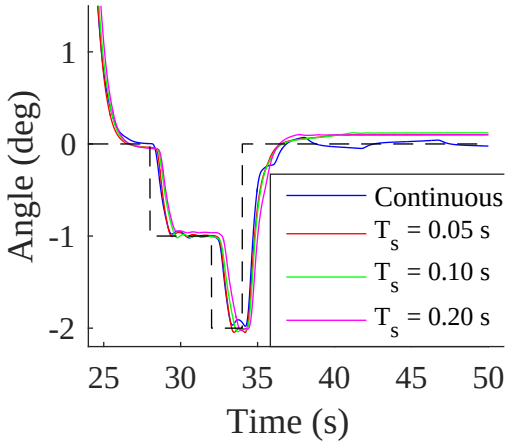

Figure 5.42: End section of the test signal, double capacitance.

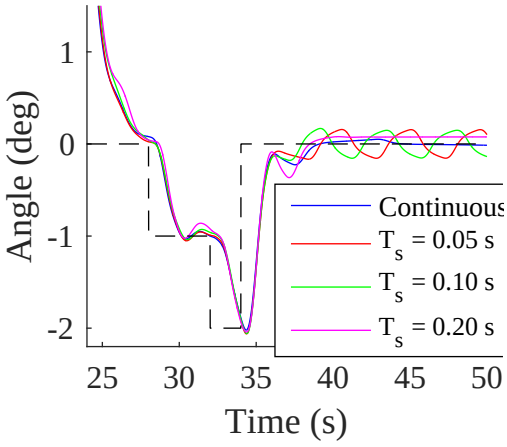

Figure 5.43: End section of the test signal, tenfold capacitance.

5.6.3 Leakage coefficient

The leakage coefficient was varied from $L = 15$ l/min/225 bar to $L = 2$ l/min/225 bar and $L = 40$ l/min/225 bar. The pole location analysis of the linearized system in Sec. 4.3 showed that variation of the leakage coefficient has the effect of changing the damping of the oscillatory poles and almost no effect to the other poles.

Reducing the leakage coefficient didn't require the modification of controllers. However, the increase from 15 to 40 l/min necessitated reducing the controller gains for $T_s = 0.20$ s: $P = 0.38 \rightarrow P = 0.35$, but not for $T_s = 0.05$ s or $T_s = 0.10$ s.

The step responses are shown in Figs. 5.44 and 5.45 and the performance during the end section of test signal in Figs. 5.46 and 5.47.

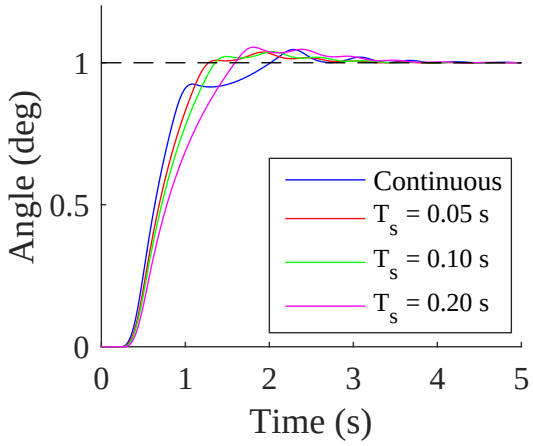

Figure 5.44: Step response, leakage rate 2 l/min / 225 bar.

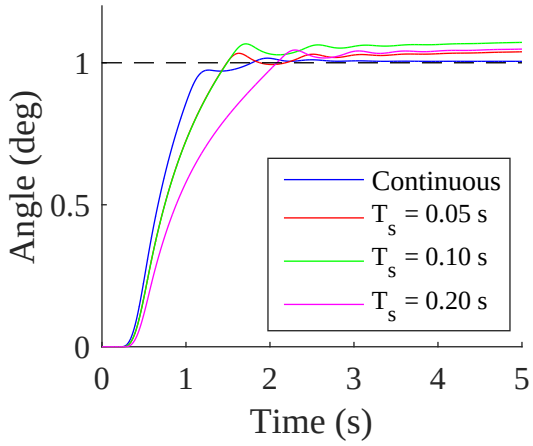

Figure 5.45: Step response, leakage rate 40 l/min / 225 bar.

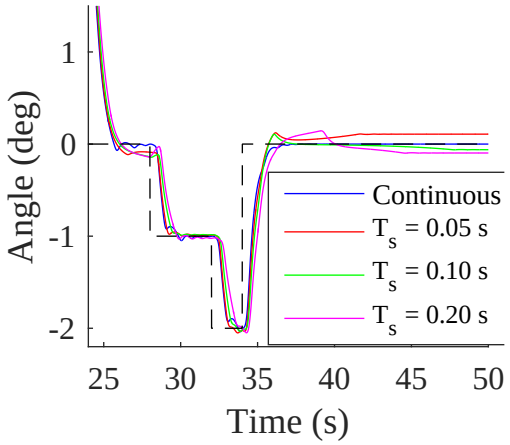

Figure 5.46: Test signal, leakage rate 2 l/min / 225 bar.

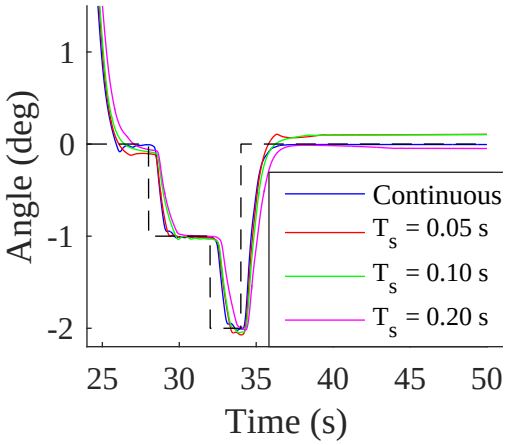

Figure 5.47: Test signal, leakage rate 40 l/min / 225 bar.

5.6.4 Pump output and motor displacement

Contrary to the rest of the parameters, the effects of varying maximum pump output K_p can be determined by simple mathematical reasoning and hence do not need to be simulated. This follows from the fact that, in the linear region, the dynamic effects caused by multiplying K_p by a certain factor are exactly canceled out by dividing the controller gains by that same factor, since

$$\mathcal{L}\{Q_p(t)\} = \mathcal{L}\{e(t)\} \cdot G_c(s)K_c \cdot K_p G_{sp}(s) \tag{5.2}$$

where $Q_p(t)$ is the pump output as a function of time, e(t) is the error signal as a function of time, $G_{sp}(s)$ is the swashplate transfer function, $G_c(s)$ is the controller transfer function and K_c is the controller gain. Hence, if pump output is doubled, halving the controller gains restores the closed-loop poles.

The effects of motor displacement variation were examined by replacing D_A by $D'_A = 0.5 \cdot D_A$. Recalling from Sec. 4.1.4 that D_A is proportional to the ratio of motor displacement and gear ratio, this substitution is equivalent to either halving

the motor displacement or doubling the gear ratio (or any other combination so that $D'_A = 0.5 \cdot \frac{D_m}{R}$).

The pole location analysis (Sec. 4.3) showed an increase in oscillation frequency of the oscillatory poles and a decrease in damping as the motor displacement was lowered. Indeed, the controller gains had to be heavily reduced in order to avoid large oscillations. Moreover, for $T_s = 0.20$ s, a P-controller didn't result in a satisfactory response. However, after replacing the controller with one that includes the previous error value (velocity approximation), all of the three controllers produced identical step responses. The controllers were

$$\begin{gathered}\text{Continuous} \rightarrow P = 0.20 \\ T_s = 0.05 \text{ s} \rightarrow P = 0.16 \\ T_s = 0.10 \text{ s} \rightarrow P = 0.14 \\ T_s = 0.20 \text{ s} \rightarrow D(z) = 0.2(1 - 1.5z^{-1})\end{gathered}$$

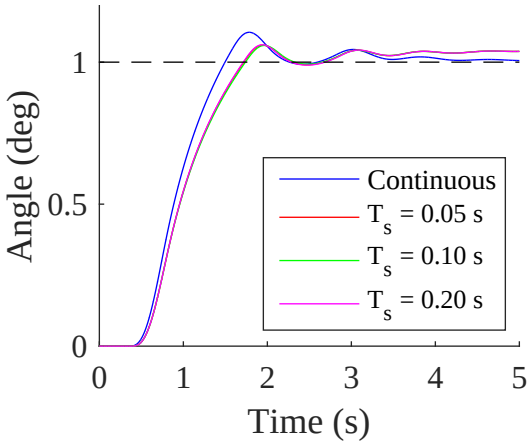

Figure 5.48: Step response, motor displacement $D'_A = 0.5 \cdot D_A$.

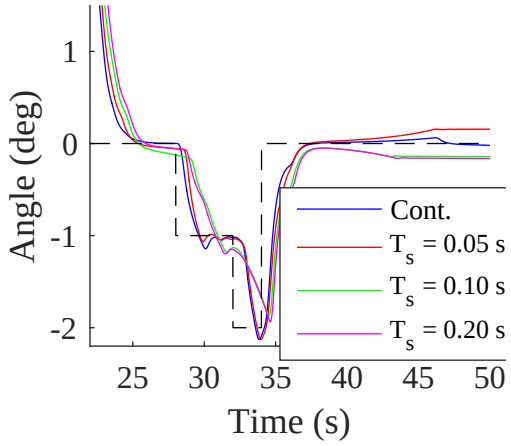

Figure 5.49: Test signal, motor displacement $D'_A = 0.5 \cdot D_A$

6 Conclusions

In this thesis, the position control of a closed-loop hydraulic system was studied by means of simulation. The position control was performed with digital and continuous controllers and the performances were compared. The sampling periods of interest were $T_s = 0.05$ s, $T_s = 0.10$ sand $T_s = 0.20$ s.

A comprehensive testing of the system was performed that consisted of the study of the effects of measurement delays and antialiasing filtering, measurement noise, external disturbances, quantization, backlash and model parameter variations. The results show that under the assumptions made in this thesis, a simple design by emulation approach yields digital controllers that result in practically equivalent performance when compared to the continuous controllers. We argue that this is mainly the result of two factors. First, the resonant poles in the closed-loop system are either highly damped or of small magnitude and can be neglected as long as the system parameters are not excessively varied. Thus, the behavior of the system can be approximated as a highly damped second-order system. The hydraulic capacitance is small enough that the system dynamics are almost entirely determined by the pump dynamics. Second, the rise time ($T_r = 1.6$ s) was permitted to be rather large relative to the system dynamics. Hence, relatively small controller gains were used. In fact, according to the step response specification, the controller gains could have been lowered even further such that $T_r = 3.0$ s. However, this was not necessary.

Dynamic effects of filtering and measurement delay. The first test aimed to investigate the effects of measurement delays T_{dm} and antialiasing filtering f_{fbp} to the dynamic behavior of the system. The step responses with measurement delays (Figs. 5.4 – 5.6) and antialiasing filtering (when controllers remained unchanged) were examined. The effects were found to be very similar, as shown in Figs. 5.7 – 5.9. This suggests that, to a reasonable accuracy and within a limited range of delays, filtering approximates the effects of measurement delays (see Sec. 2.3) and that, from a dynamic point of view, lowering the filter breakpoint corresponds to a certain increase in measurement delay. To be more precise,

$$\begin{aligned} T_{dm} = 0.05 \text{ s} &\leftrightarrow f_{fbp} = 3.3 \text{ Hz} \\ T_{dm} = 0.10 \text{ s} &\leftrightarrow f_{fbp} = 1.7 \text{ Hz} \\ T_{dm} = 0.20 \text{ s} &\leftrightarrow f_{fbp} = 0.8 \text{ Hz} \end{aligned}$$

were interchangeable when considering the step responses. To approximate the presence of measurement delays in the simulations (without increasing the number of simulations), the filter breakpoint was selected purposefully lower (2 Hz) than what would be required. A reasonable assumption is then that 2 Hz filtering approximates the behavior with, say for example, 6 Hz filtering and T_{dm} between 0.05 to 0.10 s.

Measurement noise. The effects of measurement noise were determined in terms of absolute mean amplitude, standard deviation (dispersion of the values) and maximum value. If linearity is assumed and the mean absolute amplitude of the measurement noise is varied from 1° to 2° or below 1°, these results will scale directly. (On the other hand, if pump saturations must be accounted for, the

measurement noise is clearly excessive.) The effects were found to be dependent on sampling period T_s and antialiasing filter breakpoint f_{fbp}. The results are shown in Figs. 5.15 – 5.17 and Tables 5.3 – 5.5. The difference between a continuous controller and a digital controller with $T_s = 0.05$ s, $f_{fbp} = 6$ Hz, was insignificant. It can therefore be concluded that decreasing the sampling period from $T_s = 0.05$ s does not significantly improve noise rejection when this control scheme is used. Furthermore, lowering the filter breakpoint did not yield significant benefits in terms of absolute mean and standard deviation in either case. This is understandable since $f_{fbp} = 6$ Hz provides enough attenuation at the Nyquist frequency $f_n = 10$ Hz for $T_s = 0.05$ s. However, as expected, the effect of measurement noise became more significant as the sampling period was increased and in order to maintain similar noise rejection properties, the antialiasing filter breakpoint had to be lowered (and controller gains accordingly) as the sampling period was increased from $T_s = 0.05$ s to $T_s = 0.20$ s. Even when $T_s = 0.20$ s, the noise rejection was again almost the same as with the other controllers when selecting $f_{fbp} = 2$ Hz. In this case increasing f_{fbp} from 2 Hz to 6 Hz led to 78% increase in mean absolute amplitude and 100% increase in SD, so the filter selection is more critical for larger sampling periods. In this case, the Nyquist frequency is only $f_n = 2.5$ Hz. Although the statistics were better for all of the digital controllers when $f_{fbp} = 2$ Hz, a direct comparison would not be fair since lowering the controller gain also reduces the bandwidth of the control system.

The adjusted control values next to the Figs. 5.15 – 5.17 indicate that the control system was more sensitive to changes in f_{fbp} as the sampling period is increased. When $T_s = 0.05$ s, no controller adjustments were required between $f_{fbp} = 3$ Hz and $f_{fbp} = 6$ Hz.

Torque disturbances (see Sec. 5.4) had a negligible effect on the system, even though they were conservatively modelled as a torque equivalent to 10 bar pressure (on average). Of course, the positional stiffness is in general one of the important advantages of hydraulic systems.

Quantization. The effects of quantization were only briefly examined. This can be justified by the theoretical discussion in Sec. 2.4, since quantization effects can be regarded as bounded noise in a stable system. The purpose of the simulation was to characterize the effects of this noise. The results are shown in Sec. 5.5.1. For all practical purposes, the 16-bit controller behaved as if there were no quantization. For the 10-bit controller, the statistics were similar to those of the measurement noise ($|\mu| = 1°$) and for 12-bit, comparable to $|\mu| = 1/3°$.

Backlash. The effects of backlash and the existence of limit cycles were studied in Sec. 5.5.2. All of the tested sampling periods exhibited the same limit cycle behavior (including the continuous controller with quantization). The existence of limit cycles was determined by the controller gain together with quantization interval. For 12-bit word size there was a distinct gain that determined the existence of limit cycles

$$P < 0.50 \rightarrow \text{No limit cycle}$$
$$0.50 \leq P \rightarrow \text{Limit cycle}$$

Furthermore, for all $0.50 \leq P$, the limit cycles were practically identical. That is, the amplitude was approximately $A_{LC} = 0.14°$. For 16-bit word size (practically continuous amplitude), there were no significant differences between the controllers. Torque disturbances had no effect to the existence of limit cycles and did not generate significant unwanted behavior. In fact, the mean absolute amplitude was observed to be slightly reduced. These results indicate that with appropriate selection of controller gain, backlash should not cause issues for any of the tested controllers.

Model parameter variations. Since a model is always inaccurate to some degree, it is necessary to allow variation in the parameters. Rather than to determine the sensitivity to parameter variations [i.e. fixing the controller and observing the change in response as parameters are varied (see uncompensated delays and filtering in Sec. 5.2)], our goal was to show whether there exists a well-performing digital controller for each parameter configuration. The sensitivity can be inferred based on how much the controllers were modified. This indicates that increasing the sampling period generally increased the sensitivity.

Final conclusions and recommendations. The results in Sec. 5.6 show that even when the parameters were varied, digital controllers with equivalent performance were found in each case (the only exception was limit cycles with tenfold capacitance near $\theta_A = 0°$, which did not occur in the step responses). As a final conclusion, the results indicate that a simple digital control system (sampling periods $T_s = 0.05$ s, $T_s = 0.10$ s and $T_s = 0.10$ s) is sufficient to provide performance equivalent to that provided by a continuous P-controller. The results suggest also that lowering the sampling period alone (from $T_s = 0.05$ s) is unlikely to result in improved performance. However, if superior performance is desired there are several options. These options include using more advanced control algorithms (e.g. Kalman filter and pole placement), using a higher-order antialiasing filter with better frequency response and increasing the computer and converter word sizes. The control methods and filtering that were considered in this thesis were simple, yet with proper controller adjustments provided practically the equivalent performance.

References

[1] Dorf, R. C. and Bishop, H. B. *Modern Control Systems.* 12th ed. New Jersey, Prentice Hall, 2011.

[2] Franklin, G. F., Powell, J. D. and Workman, M. L. *Digital control of dynamic systems.* 3rd ed. Menlo Park, Addison-Wesley, 1998.

[3] Åstrom, K. J. and Wittenmark, B. *Computer-Controlled Systems. Theory and Design.* 3rd ed. New Jersey, Prentice Hall, 1997.

[4] Ellis, G. *Control System Design Guide.* 4th ed. Oxford, Elsevier, 2012.

[5] Oppenheim, A. V., Schafer, R. W. and Buck, J. R. *Discrete-Time Signal Processing.* 2nd ed. New Jersey, Prentice Hall, 1999.

[6] Couch, L. W. *Digital and Analog Communication Systems.* 7th ed. New Jersey, Prentice Hall, 2007.

[7] Ackerman, J. *Sampled-Data Control Systems.* Berlin, Springer-Verlag, 1985.

[8] Ogata, K. *Discrete-time Control Systems.* 2nd ed. New Jersey, Prentice Hall, 1995.

[9] Smeds, K. and Lu, X. Effect of sampling jitter and control jitter on positioning error in motion control systems. *Precision Engineering*, 2012, vol. 36, no. 2, pp. 175–192.

[10] Fadali, M. S. and Visioli, A. *Digital Control Engineering : analysis and design.* 2nd ed. Oxford, Elsevier, 2013.

[11] Hirata, H. and Powell, J. D. Sample Rate Effects on Disturbance Rejection for Digital Control Systems. *American Control Conference*, 1990, pp. 1137–1145.

[12] Peled, U., and Powell, J. D. The Effects of Prefilter Design on Sample Rate Selection in Digital Control Systems. *Proc. of AIAA GC Conference*, 1978, Paper No. 78-1308.

[13] Delta Computer Systems. RMC75 Motion Controller. Retrieved November, 30, 2015 from http://deltamotion.com/products/motion/rmc70/.

[14] National Instruments. Motion Control. Retrieved November, 30, 2015 from http://www.ni.com/motion/.

[15] Higham, N. J. *Accuracy and stability of numerical algorithms.* 2nd ed. Philadelphia, Society for Industrial and Applied Mathematics, 2002.

[16] Widrow, B. Statistical Analysis of Amplitude-Quantizaed Sampled-Data Systems. *AIEE Transactions on Applications and Industry*, 1961, pp. 1–14.

[17] Bertram, J. E. The Effect of Quantization in Sampled-Feedback Systems. *AIEE Transactions on Applications and Industry*, vol. 774, no. 4, 1958, pp. 177–182.

[18] Golnaraghi, F. and Kuo, B. C. *Automatic Control Systems.* 9th ed. New Jersey, John Wiley & Sons, 2010.

[19] Merritt, H. E. *Hydraulic Control Systems.* New York, John Wiley & Sons, 1967.

[20] Vidyasagar, M. *Nonlinear Systems Analysis.* 2nd ed. New Jersey, Prentice Hall, 1993.

[21] Banks, S. P. *Control Systems Engineering. Modelling and Simulation, Control Theory and Microprocessor Implementation.* London, Prentice Hall, 1986.

[22] Piskunov, N. *Differential and Integral Calculus II.* 2nd ed. Moscow, Mir Publishers, 1974.

[23] Prasetiawan, E. A. Modeling, simulation and control of an earthmoving vehicle powertrain simulator. Master's Thesis, University of Illinois at Urbana-Champaign, Urbana, Illinois, 2001.

[24] Kavanagh, G. P. Dynamic Modelling of an Axial Piston Hydraulic Pump. Master's Thesis, University of Saskatchewan, Saskatoon, 1987.

[25] Akkaya, A. Effect of bulk modulus on performance of a hydrostatic transmission control system. *Sadhana*, 2006, vol. 31, no. 5, pp. 543–556.

[26] Fonselius, J., Rinkinen, J. and Vilenius, M. *Koneautomaatio. Hydrauliikka II.* 2nd ed. Helsinki, Oy Edita Ab, 1997.

[27] Mandal, S. K., Singh, A. K., Verma, Y. and Dasgupta, K. Performance Investigation of Hydrostatic Transmission System as a Function of Pump Speed and Load Torque. *Journal of The Institution of Engineers (India): Series C*, 2012, vol. 93, no. 2, pp. 187–193.

[28] Pršić, D., Nedić N. and Dubonjić, L. Modeling and Simulation of Hydraulic Long Transmission Line by Bond Graph. *Journal of Mechanics Engineering and Automation*, 2013, vol. 3, pp. 257–262.

[29] Nedić, N. N., Filipović, V. Z. and Dubonjić, L. M. Design of Controllers With Fixed Order for Hydraulic Control System With a Long Transmission Line. *FME Transactions*, 2010, vol. 38, pp. 79–86.

[30] Jelali, M. and Kroll, A. *Hydraulic Servo-systems : modelling, identification and control.* London, Springer, 2003.

[31] Watton, J. *Fluid power systems: modeling, simulation, analog and microcomputer control.* Cambridge, Prentice Hall, 1989.

[32] Kauranne, H., Kajaste, J. and Vilenius, M. *Hydraulitekniikka.* 2nd ed. Helsinki, Sanoma Pro Oy, 2013.